Investigation of Factors that Influence Wind-Tunnel Modelling in Vehicle Thermal Simulation

Arun Kumar

Master of Science Thesis

TU Delft Delft University of Technology

VOLVO CAR GROUP

Investigation of Factors that Influence Wind-Tunnel Modelling in Vehicle Thermal Simulation

Master of Science Thesis

For the degree of Master of Science in Aerospace Engineering - Aerodynamics at Delft University of Technology

Arun Kumar

10-06-2016

Faculty of Faculty of Aerospace Engineering(LR) · Delft University of Technology

The work in this thesis was supported by Volvo Cars Group. Their cooperation is hereby gratefully acknowledged.

TU Delft Delft University of Technology

DELFT UNIVERSITY OF TECHNOLOGY

FACULTY OF AEROSPACE ENGINEERING

DEPARTMENT OF AERODYNAMICS AND WIND POWER

AERODYNAMICS GROUP

GRADUATION COMMITTEE

Dated: 24th February 2014

Committee chairman:

Prof.dr. Stefan Hickel

Committee members:

Prof.dr. Alexander van Zuijlen

Prof.dr. Axelle Vire

Abstract

Technological advancements in computational simulations have reduced our dependence on physical testing. The automotive industries aim to minimize physical testing and increase the use of computational simulations. They are effective both in terms of man hours and cost of product development. Volvo Cars Group is thus having an ongoing project on developing a Virtual Wind Tunnel. The objective of the thermodynamics team is to build a Virtual Wind Tunnel Simulation where the physical testing is no longer a part of development but for final validation.

This assignment plays an important role in this project. The factors that significantly influence thermal simulations are investigated in this work. Exhaust suction pipes, wheel rotation, involvement of Moving Reference Frame for wheel rims and ride height fluctuations are the factors considered in this thesis. The model under study is Volvo S60. The reference model considered is a smaller domain of the wind tunnel and the rear half of the vehicle. This model is referred to as the reference model and later used to implement each factor and obtain a first order result. This model consists of certain points of measurements called thermocouple points which are used as temperature reading points. Their coordinates are the same as the thermocouples used in the experimental wind tunnel test. Different modifications are made on the reference model to bring out model with exhaust suction pipes, model with reduced ride height, model with wheel rotation and model with wheel rotation and MRF on rims. ANSA software is used for CAD cleaning and modifications. The final model from ANSA is then converted as a NASTRAN file which is readable for STARCCM+. STARCCM+ is used as mesher and CFD-solver.

The heat source in these models is the exhaust system, providing a constant heat output. For simulation the boundary conditions of the domain which includes inlet, sides and top are taken from a converged solution of a full model simulation. This adaptation is made for faster convergence and more accurate boundary predictions. The simulation began with a reference model and its converged solution is used as an initial condition to the remaining models for a faster converged solution. Final results from thermocouple points are compared with the reference model. Logical explanations for respective occurrence are derived using different field functions such as convective heat transfer, radiation, temperature, velocity etc.

It is found that all the factors chosen have notable influence over the domain under study. The parts highly influenced are the exhaust system and the heat shield. Among them, the influence of exhaust suction pipes is seen to be more profound. The end result of the thesis recommends that the exhaust suction pipes be taken into account when it comes to wind-tunnel modelling and also wheel rotation with MRF on rims when it comes to modelling the real road physical test. This thesis also emphasis the need to focus further on evaluating the influence of different rim profiles and development and optimization of the exhaust suction pipes.

Table of Contents

List of Figures

Acknowledgements

I would like to express my sincerest gratitude to all those who were involved in my thesis work and guided me throughout the study and research.

I would like to thank my principal supervisors, Begoña León Moya and Jacob Vikström for providing me with the opportunity to work on this visionary project. They were always a constant source of guidance, inspiration, and motivation. Their assistance and support throughout my work were priceless.

I would like to thank my university supervisor Prof.dr.ir. Stefan Hickel for his critical evaluation of my work and guidance in order to meet the requirements of the university. His suggestions and feedback during the progress meetings proved to be an important source of inspiration and motivation throughout the thesis.

I take this opportunity to thank Mats Löfman, manager of Volvo Cars thermodynamics department, for providing all the necessities both technical and administrative support. I am grateful to Emil Willeson for sharing the CAD models and full model simulation results. I am extremely grateful to Niklas Löfgren for his patience and commitment in helping me with STARCCM+ in spite of his busy schedule.

Finally, I would like to thank my parents and sister, who have supported me through thick and thin to follow my dreams, even if that involved moving to the other side of the world. They have been there to help me through all the challenges along the way and I certainly would not have made it this far without them.

Delft, University of Technology — Arun Kumar
10-06-2016

List of Symbols and Abbreviations

Abbreviations

CFD	Computational Fluid Dynamics
CFL	Courant Friedrichs Lewy condition
CPU	Central Processing Unit
MRF	Moving/Multiple Reference Frame
$RANS$	Reynolds-Averaged Navier-Stokes
LES	Large eddy simulation
DES	Detached eddy simulation

Greek symbols

α_{R_A}	Absorptivity of surface A	$-$
ϵ_R	Emissivity	$-$
ϵ	Dissipation rate of turbulence kinetic energy	$\frac{J}{kgs}$
γ	Specific heat ratio	$-$
μ	Dynamic viscosity	$\frac{kg}{ms}$
μ_t	Eddy viscosity	$\frac{kg}{ms}$
ν	Local kinematic viscosity	$\frac{m^2}{s}$
$\overline{\Omega_{ij}}$	Mean rate-of-rotation tensor	$\frac{rad}{s}$
ω_k	Angular velocity	$\frac{rad}{s}$
ρ	Density	$\frac{Kg}{m^3}$
$\bar{\rho}$	Mean density	$\frac{Kg}{m^3}$
σ	Turbulent Prandtl-Schmidt number	$-$
σ_k	Prandtl-Schmidt number for k	$-$
σ_{SB}	Stefan-Boltzmann Constant	$\frac{W}{m^2T^4}$
τ_{ij}	Reynolds stress tensor	$\frac{Kg}{ms}$

[H] **Roman symbols**

C_f	Skin friction coefficient	$\frac{W}{m^2K}$
E_R	Emissive power	$\frac{W}{m^2K}$
E_{R_b}	Emissive power of black body	$\frac{W}{m^2K}$
e	Specific internal energy	$\frac{J}{Kg}$
$\tilde{e}$	Mean specific internal energy	$\frac{J}{Kg}$
H	Total enthalpy	$\frac{J}{kg}$
h	Specific enthalpy	$\frac{J}{kg}$
$\tilde{h}$	Mean specific enthalpy	$\frac{J}{kg}$
h	Convective heat transfer coefficient	$\frac{W}{m^2K}$
k	Thermal conductivity	$\frac{W}{m^2K}$
k	Specific turbulent kinetic energy	$\frac{J}{Kg}$
k_{cond}	Local conductive heat transfer coefficient	$\frac{W}{m^2K}$
M	Molecular weight	$\frac{g}{mol}$
P_{abs}	Absolute Pressure	Pa
$P_{abs_{total}}$	Absolute Total Pressure	Pa
P_{Ref}	Reference Pressure	Pa
P_{Static}	Static Pressure	Pa
P_{total}	Total Pressure	Pa
q	Heat flux density	$\frac{W}{m^2}$
$q_{rad_{net}}$	Net radiant heat flux	$\frac{W}{m^2}$
q_{cond}	Local conductive heat flux	$\frac{W}{m^2}$
q_{conv}	Local convective heat flux	$\frac{W}{m^2}$
R	Specific gas constant	$\frac{J}{kgK}$
Re	Reynolds number	$-$
Re_y	Wall-distance-based Reynolds number	$-$
R_u	Universal gas constant	$\frac{J}{KmolK}$
T	Temperature	K
T_{fluid}	Fluid temperature close to surface	K
T_S	Surface temperature of Solid	K
t	Time	s
$\bar{t}_{ij/ji}$	Mean viscous stress tensor	Pa or N/m^2
u	Flow velocity	$\frac{m}{s}$
u^+	Dimensionless flow velocity	$-$
$u'_{i/j}$	Fluctuating flow velocity	$\frac{m}{s}$
$\tilde{u_{i/j}}$	Mean flow velocity	$\frac{m}{s}$
u_τ	Friction velocity	$\frac{m}{s}$
v	Velocity	$\frac{m}{s}$
x	Displacement	m
y	Distance to the nearest wall	m
y^+	Dimensionless wall distance	$-$

Chapter 1

Introduction

1-1 Background

The automotive industry still rely heavily on physical testing for validation and verification. In the present era of computation and virtual simulations the industries are pushing their limits to minimize that dependency on physical testing through more robust computational models. Environment and Fluid Engineering Department at Volvo Cars also embraces that vision by currently developing a virtual wind tunnel to support the product development. These virtual designs will be used to predict the evolving characteristics of the given physical system using CFD simulations. Coupled with high-performance computing, virtual design offers fast and reliable testing of complete vehicle, and identification of critical regions. One of the main challenges involved in this vision is the correlation of results of thermodynamics physical testing to CFD simulations. The thermodynamics division is interested in studying the factors that could alter their computational results causing deviation from their wind tunnel results. This is a wide field to look into, hence prioritizing the potential contributors to this deviation is vital.

Recently the field of thermal management has been focusing persistently on high performance engines along with controlled climate systems making engineers encounter design challenges such as geometry and constricted underhood space [1]. This leads to designing complex cooling systems which includes complex airflows and air path designs though required components underhood [2, 3, 4]. A close study of such flows is almost impractical through experimental methods due to both technical and financial reasons and thus engineers rely on CFD simulations. Hence a reliable simulation solution is inevitable. According to M. Khaled et al. [5] even small elevations ranging from 0.5 to 1.5 cm between front and rear of a vehicle affects internal airflow resulting upto 20% temperature rise around underhood components. Thus shows the importance of focusing on aero-thermal phenomena. With current constrains such as constant augmentation of engine specific power, increase in reliability, compactness and demand of cost reduction result in limiting the dependency of high thermal resistive metals, the vital components that are vulnerable to thermal failure can only be protected by complex

air cooling systems. To design such a system, the dependence on CFD simulation is significant since the costs involved with physical tests are high.

Looking into design and development management, building a product with efficient simulation which provides accurate and robust early detection of issues in the design phase is inevitable. It also helps in developing related counter measures even before building a prototype reduces the dependency of physical tests to just final verification. Reduction in the numerous physical tests and building a more accepted first hand prototype is an obvious choice for a robust, cost effective and efficient methodology. The wind tunnel could never simulate a real road environment due to some parameters. The dominant ones are referred in 1-2. Studying these parameters and their influences can bring alternative solutions to counter act the same.

1-2 Objectives of this Thesis Work

As the heading of this thesis reveals, the aim of this research work is to study the influential parameters involved in the wind tunnel models that might possibly affect the results when correlated to CFD simulations and real road conditions. In this assignment four parameters are considered for detailed investigation.

The thermal department requires a detailed study about the aerodynamic influences in heat transfer. Many researches have been conducted on the regions such as engine bay, heat exchangers, air inlet and outlet geometry, and design. However, when it comes to the flow underneath the vehicle and the exhaust system, the aerodynamic influences are seldom studied. Keeping these key points in mind the author is able to propose the aims and objectives entitling the final research question.

The main research question aimed to be solved in this research is :

What are the factors in wind-tunnel modelling that have potential influence on heat transfer underneath the vehicle? In addition, how can the effects subjective to the specific wind tunnel of Volvo Cars, be taken into in this research and validated?

Time constraint and height of interest on certain regimes limits to only solve four significant sub questions among many:

- **Is the influence of the under pressure present in the exhaust suction pipes that are attached to the wind tunnel an important factor?**
  Unlike the aerodynamic tests the thermodynamic tests take place with the engine running. It is important that no exhaust gas is emitted freely into the wind tunnel. Thus the suction pipes have an under pressure to suck the exhaust gases coming out of the exhaust pipes. This will change the flow physics of the gas close to this region and further upstream. But the extend of its influence is not yet quantified for this wind tunnel. In this system two pipes are provided, protruding from the floor are attached

to the exhaust pipes of the vehicle. This suction can affect the flow close to the muffler. It is important to see the extend of its influence.

- **Is the influence of the rim rotation over the airflow underneath the vehicle significant?**
  It is clear from studies that the wheels and rims influence the total vehicle drag [6, 7, 8, 9]. However there have not been any studies on their influence on heat transfer rate. The disturbed air from the rims does promise some significant influence on the flow characteristics underneath the vehicle both laterally and longitudinally.
- **Is the influence of the wheel rotation over the airflow underneath the vehicle significant?**
  In the physical wind tunnel thermal simulation the rear wheels are stationary. Hence the absence of the rear wheel rotation in physical wind tunnel testings needs to be investigated to compare with the real road simulation where the air flow due to the wheel rotation is potentially disturbed.
- **How are the flow conditions under the vehicle at different ride heights?**
  According to the results from Volvo Cars they are able to discover a significant temperature difference with variation of ride height . However the reason has note been derived so far leaving it as an important research sub-question in this thesis.

It is clear from these objective questions that the important result that should be obtained is a three-dimensional flow visualization underneath the vehicle. The flow should be visualized for the above mentioned factors and respective flow patterns observed. Through analysing these flow patterns some conclusions regarding the influences over different parameters can be deduced.

This research is taking place under the thermodynamics team of Volvo Cars after inspecting the current wind tunnel design, testing methods and researches achieved so far.

1-3 Layout of the Thesis

Chapter 2 provides an introduction to physics with section 2-1 defining modes of heat transfer and section 2-2 later leading to the theoretical aspects of different models chosen for this simulation. Finally section 2-4 explains in detail regarding different possible cell meshers and the reason for choosing a particular continua.

Chapter 3 vividly guides through the vehicle and the domain under study. It explains the different parts that are distinguished in the model.

Chapter 4 provides the total detail of the model with wheel rotation and with and without MRF on rims. Section 4-1 provides the detailed observations and reasoning for the respective occurrences. Section 4-2 concludes with importance of this parameter and the individual contribution of wheel rotation and MRF on rims.

Chapter 5 provides the detail of the model with exhaust suction pipes. It begins with defining the model and the experimental method adapted for calculating the mass flow rate created

by the exhaust suction pipes. Section 5-1 provides the detailed observations and reasoning for the respective occurrences.

Chapter 6 provides the influence of ride height variation using the model with reduced ride height. Section 6-1 briefly describes the results and reasoning for the respective occurrence. The reasoning is focused mainly on the important regions.

Chapter 7 reveals potential limitations that can be found in this research and need further looked into. It provides a summarised conclusion and suggestions from the detailed study of chapter 4, 5 and 6 for future research.

Chapter 2

Theoretical Basics and Modelling

Computational Fluid Dynamics, CFD, is the tool used for simulations in this thesis. It is the branch of fluid dynamics that uses algorithms and numerical analysis to simulate the interactions of gases and liquids. Provided with boundary conditions, using computers for calculations, it solves and visualizes the problems related to fluid flows.

2-1 Heat Transfer

This thesis is primarily focused on the study of heat transfer and thermal simulation. Heat transfer is the study of heat/energy transfer from one medium to another or within the medium depending on the temperature gradient. There are three modes of heat transfer and they are:

1. Conductive heat transfer
2. Convective heat transfer
3. Radiative heat transfer

2-1-1 Conductive Heat Transfer

Conductive heat transfer is defined as the flow of internal energy by interaction of the adjacent particles from a region of higher temperature to a region of lower temperature. This mode of heat transfer is present in solids, fluids and plasmas. In solids the conduction is greater compared to other states of matter as atoms are relatively tightly packed thus have close fixed spacing. In fluids the conduction is due to collision of more energetic particle and the molecule diffusion during random motion. The Fourier's law or law of heat conduction explains the relation of local heat flux with temperature gradient as shown in equation 2-1. [10]

$$q_{cond} = -k_{cond}\frac{\partial T}{\partial x} \tag{2-1}$$

where, q_{cond} is local conductive heat flux, $-k_{cond}$ is local conductive heat transfer coefficient, ∂T is surface temperature difference between measured points and ∂x is distance between the respective points.

The negative sign in the equation represent the direction of energy flow, i.e, from high temperature region to low temperature region.

2-1-2 Convective Heat Transfer

When the energy transfer takes place due to the movement of fluids it is called convective mode of heat transfer. This mode of heat transfer comprises of two mechanisms. The mechanism where the energy transfer occurs due to random molecular motion called diffusion and the mechanism called as advection where energy transfer occurs due to the collective molecular motion / large-scale bulk fluid motion. The heat transfer due to diffusion is dominant at the interface between solid and fluid. This is because at the interface the relative motion between fluid molecules and surface is zero. Convection can either be natural or forced. In this case effect of the natural convection is negligible. Convective heat transfer at a surface is determined by Newton's law of cooling as shown by equation 2-2. [10]

$$q_{conv} = h(T_S - T_{fluid}) \tag{2-2}$$

where, q_{conv} is local convective heat flux, h is local convective heat transfer coefficient, T_S is surface temperature of solid and T_{fluid} is the fluid temperature close to surface.

2-1-3 Thermal Radiation

All matter that has a temperatures greater than absolute temperature emits electromagnetic waves. In this electromagnetic wave spectrum the waves falling in the wavelength between $0.1\mu m$ and $100\mu m$ fall in the thermal radiation spectrum. In this heat transfer mechanism the thermal energy in converted to electromagnetic energy. [11]

The thermal radiation does not require any medium for heat transfer and it transfers the fastest in vacuum. In the case of solids and liquids the radiations emitted by inner molecules are absorbed by the neighbouring molecules. Thus in effect the emitted radiations from solid or liquid mediums are originated from molecules near the surfaces. This makes the emission as a surface phenomena. The emissive power from a real surface is given by equation 2-3.

$$E_R = \epsilon_R \cdot \sigma_{SB} \cdot T_S^4 \tag{2-3}$$

$$\epsilon_R = \frac{E_R}{E_{R_b}} \tag{2-4}$$

where, E_R is emissive power of the real surface, E_{R_b} is emissive power of the black body, σ_{SB} is the Stefan-Boltzmann Constant, ϵ_R is emissivity of the respective surface and T_S is surface temperature of solid.

When radiation is incident upon a surface, a fraction is reflected, a fraction is absorbed and the remaining is transmitted through the material as shown in equation . This reflectivity, absorptivity and emissivity of radiation depends on the emission angle, surface temperature, wavelength of the radiation and surface roughness. When two infinite plates with surface A and B are considered, the net radiant heat flux emitted from surface A is given by equation 2-5.

$$q_{rad_{net}} = (\epsilon_{R_A} \cdot \sigma_{SB} \cdot T_{S_A}^4) - (\alpha_{R_A} \cdot \epsilon_{R_B} \cdot \sigma_{SB} \cdot T_{S_B}^4) \tag{2-5}$$

where, $q_{rad_{net}}$ is the net radiant heat flux, ϵ_{R_A} and ϵ_{R_B} are emissivity, T_{S_A} and T_{S_B} are temperatures of surfaces A and B respectively and α_{R_A} is the absorptivity of surface A.

2-2 Fluid Model

For the CFD simulation air is considered as an ideal gas. In the outer domain of the wind tunnel the boundary conditions input normal dry air as mentioned. However, since the exhaust system is considered as the heat source in this simulation the presence of the exhaust gas is inevitable. Hence its properties should be included at the respective regions through boundary conditions.

The solver model used for this CFD simulation is as follows:

- Three Dimensional
- Ideal gas
- Coupled solver/Flow model
- Coupled energy
- Reynolds-Averaged Navier-Stokes (RANS) equations
- $k - \epsilon$ Turbulent model
- Realizable $k - \epsilon$ Two-Layer
- Two-Layer All y^+ wall Treatment
- Radiation : Surface to surface model and Grey thermal radiation body model
- Multi-gas component : Air and exhaust gas

2-2-1 Three Dimensional

The model of study has a complex geometry hence use of a simple two dimensional figure would not capture the flow behaviour of the air involved in this geometry. Minimizing the number of cells adds to the advantage of reduced CFD simulation time. This raises a logical question of using a bisected model of the given geometry using the symmetry plane, i.e, XZ plane through the origin. However this geometry is not completely symmetric along XZ axis as it is clear from the fig 3-2.

2-2-2 Ideal Gas

All gases that behave according to the Kinetic Molecular Theory are Ideal gases. Therefore when dealing with ideal gases the Ideal gas equation is used to relate all the parameters needed to solve a problem, as shown in equation 2-6. [12]

$$\rho = \frac{P_{abs}}{RT} \tag{2-6}$$

where,

$$P_{abs} = P_{Static} + P_{Ref} \tag{2-7}$$

and

$$R = \frac{R_u}{M} \tag{2-8}$$

where,

Universal gas constant, $R_u = 8314.4621 \frac{J}{KmolK}$, P_{abs} is absolute pressure, P_{Static} is static pressure, P_{Ref} is reference pressure, T is temperature and M is molecular weight.

Also it is important to note that the absolute total pressure $P_{abs_{total}}$ is the sum of total pressure reading in the STARCCM+, i.e, total pressure P_{total} and reference pressure P_{Ref} :

$$P_{abs_{total}} = P_{total} + P_{Ref} \tag{2-9}$$

It is clear that no gas is truly ideal in real world. Two major assumptions required to make a gas ideal are:

- There are no intermolecular forces acting among the particles.
- The atomic volume occupied by the particles are ignored, i.e, they are considered as point masses. [13]

2-2-3 The Coupled Flow Model

The Coupled Flow Model uses pseudo-time marching approach solving simultaneously the equations for mass conservation and for momentum conservation. The reason for choosing this model is because of the following reasons: [14]

1. In this research, the flow consists of dominant source terms such as heat source and rotation with compressible flows in the exhaust system. In such conditions the coupled algorithm of this Coupled Flow Model provides more robust solutions.
2. Coupled Flow Model has a linear relation when it comes to CPU time consumption over number of cells, this implies that the convergence and the number of iterations required for solving are independent of mesh size.
3. When coupled with implicit solver one can apply very large CFL (Courant Friedrichs Lewy condition) number.

However it uses more memory than segregated algorithm. The computational resources provided here are enough to neglect this disadvantage. When there is presence of energy in the flow, the flow model also adds the equation for conservation of energy into the list of equations to be solved.

2-2-4 Reynolds-Averaged Navier-Stokes (RANS)

In this study all CFD simulation flows use Reynolds-Averaged Navier-Stokes (RANS) equation approach for turbulence. The logic behind the RANS approach is to separate the instantaneous pressure and velocity fields in the Navier-Stokes equation into the mean component and the fluctuating component. When the flow becomes compressible the original form of equation is altered from time average method, involving density fluctuations. In such cases the time averaging method weighed over mass is adapted, called as Favre time averaging. The mean values are obtained by density weighted time (Favre) average method for steady state condition and ensemble average method for repeatable transient condition. This results in a model of governing equations as follows: [15]

$$\frac{\partial(\bar{\rho}\tilde{u}_i)}{\partial x_i} = 0 \tag{2-10}$$

$$\frac{\partial(\bar{\rho}\tilde{u}_i\tilde{u}_j)}{\partial x_j} = -\frac{\partial \bar{P}}{\partial x_i} + \frac{\partial \bar{t_{ij}}}{\partial x_j} - \frac{\partial(\overline{\rho u_i' u_j'})}{\partial x_j} \tag{2-11}$$

$$\frac{\partial}{\partial x_j}\left[\bar{\rho}\tilde{u_j}(\tilde{h} + \frac{1}{2}\tilde{u_i}\tilde{u_i}) + \tilde{u_j}\frac{\overline{\rho u_i' u_i'}}{2}\right] = \frac{\partial}{\partial x_j}\left[\tilde{u_i}(\bar{t_{ij}} - \overline{\rho u_i' u_j'}) - \bar{q} - \overline{\rho u_j' h'} + \overline{t_{ji} u_i'} - \overline{\rho u_j' \frac{1}{2} u_i' u_i'}\right] \tag{2-12}$$

where,

$$\bar{P} = (\gamma - 1)\bar{\rho}\tilde{e} \tag{2-13}$$

and,

$$t_{ij} = \mu(\frac{\partial \tilde{u_i}}{\partial x_j} + \frac{\partial \tilde{u_j}}{\partial x_i} - \frac{2}{3}\frac{\partial \tilde{u_k}}{\partial x_k}\delta_{ij}) \tag{2-14}$$

Where, $\bar{\rho}$ is mean density, $\tilde{u}_{i/j}$ is mean velocity, $\bar{P}$ is mean pressure, $u'_{i/j}$ is fluctuating velocity, $\bar{t}_{ij/ji}$ is mean viscous stress tensor, $\tilde{e}$ is mean specific internal energy, γ is specific heat ratio, $\tilde{h} = \tilde{e} + \frac{\bar{P}}{\bar{\rho}}$ is mean specific enthalpy and $\bar{q}$ is the mean heat flux vector. In these resulting equations the term $-\overline{\rho u'_i u'_j}$ is called as Reynolds stress tensor, also denoted as $\bar{\rho}\tau_{ij}$.

2-2-5 $k-\epsilon$ Turbulent model

The selection of turbulence modelling depends on the characteristics of the flow. In this model the flow contains heat transfer and potential recirculation due to the complex geometry. In addition the CFD simulation should be robust along with high accuracy and lower computational expense. The $k-\epsilon$ Turbulent model satisfies all the above requirements. It is the most industrially accepted turbulence model.[16]
To begin with from the equations 2-11 and 2-12 the Reynolds stress tensor is related to mean velocities by employing the Boussinesq hypothesis:

$$\bar{\rho}\tau_{ij} = -\overline{\rho u'_i u'_j} = \mu_t(\frac{\partial \tilde{u_i}}{\partial x_j} + \frac{\partial \tilde{u_j}}{\partial x_i} - \frac{2}{3}\frac{\partial \tilde{u_k}}{\partial x_k}\delta_{ij}) - \frac{2}{3}\bar{\rho}k\delta_{ij} \tag{2-15}$$

where δ_{ij} is the Kronecker delta function and the eddy viscosity μ_t is given by

$$\mu_t = \frac{\bar{\rho}C_\mu k^2}{\epsilon} \tag{2-16}$$

The $k-\epsilon$ Turbulent model is a two equation model solving transport equations for both turbulence kinetic energy k and its dissipation rate ϵ as shown in equations 2-17 and 2-18.

The k equation is given by

$$\frac{\partial(\bar{\rho}\tilde{u_j}k)}{\partial x_j} = \frac{\partial}{\partial x_j}\left[(\mu + \frac{\mu_t}{\sigma_k})\frac{\partial k}{\partial x_j}\right] + \tau_{ij}\frac{\partial \tilde{u_i}}{\partial x_j} - \bar{\rho}\epsilon \tag{2-17}$$

the ϵ equation is given by

$$\frac{\partial(\bar{\rho}\tilde{u_j}\epsilon)}{\partial x_j} = \frac{\partial}{\partial x_j}\left[(\mu + \frac{\mu_t}{\sigma_\epsilon})\frac{\partial \epsilon}{\partial x_j}\right] + C_{\epsilon 1}\frac{\epsilon}{k}\tau_{ij}\frac{\partial \tilde{u_i}}{\partial x_j} - C_{\epsilon 2}\bar{\rho}\frac{\epsilon^2}{k} \tag{2-18}$$

Where, μ is the dynamic viscosity and the closure coefficients, $C_{\epsilon 1}$, $C_{\epsilon 2}$, C_μ, σ_k and σ_ϵ are given default values [17, 18].

2-2-6 Realizable $k-\epsilon$ Two-Layer

The computation in this approach is divided into two layers. First one is the layer next to the wall where the turbulent viscosity k and the turbulent dissipation rate ϵ are assigned as functions of wall distance. While the remaining region is considered as the second layer. Here the value of turbulent dissipation rate ϵ is obtained from the transport equation away from the wall but blended smoothly when it comes to near-wall layers. The turbulent viscosity k is solved for the entire flow using the equation 2-17. In this model the turbulent dissipation rate ϵ transport equation is modified [19]. As the coefficient C_μ is no longer considered constant as in the standard model [20]. It is now a function of turbulence properties and mean flow. Thus this model has new formulation for turbulent viscosity μ_t. It is clear from the name of the model, "Realizable" that this model consistent with the physics of turbulent flows satisfies certain mathematical constraints on the Reynolds stresses. This model exhibits superior performance on flow conditions involving separations, recirculation, boundary layers with adverse pressure gradients and flow rotation.

$$\mu_t = \frac{\bar{\rho} C_\mu k^2}{\epsilon}$$

Here,

$$C_\mu = \frac{1}{(A_0 + A_S \frac{kU^*}{\epsilon})} \tag{2-19}$$

provided,

$$U^* = \sqrt[2]{S_{ij}S_{ij} + \tilde{\Omega}_{ij}\tilde{\Omega}_{ij}}$$

$$\tilde{\Omega}_{ij} = \Omega_{ij} - 2\epsilon_{ijk}\omega_k \qquad \Omega_{ij} = \overline{\Omega_{ij}} - \epsilon_{ijk}\omega_k$$

$$A_0 = 4.04 \qquad A_s = \sqrt[2]{6}\cos(\phi)$$

$$\phi = \tfrac{1}{3}\cos^{-1}(\sqrt{6}W) \qquad W = \frac{S_{ij}S_{jk}S_{ki}}{\tilde{S}^3}$$

$$\tilde{S} = \sqrt{S_{ij}S_{ij}} \qquad S_{ij} = \tfrac{1}{2}\left(\frac{\partial u_j}{\partial x_i} + \frac{\partial u_i}{\partial x_j}\right)$$

Where $\overline{\Omega_{ij}}$ is the mean rate-of-rotation tensor viewed in a rotating reference frame with the angular velocity ω_k.

2-2-7 Two-Layer All y^+ wall Treatment

A mesh over a domain is considered to be successful in a computational project only if it is optimized between an acceptable accuracy and time (cost). Its importance is eminent when it comes to the affect over turbulent flows in the presence of walls. The regions near the walls, being the viscous-effected regions, the solution variables have high gradients. In order to correctly predict the turbulent flows along these walls an accurate presentation of the near wall is important. Use of wall y^+ is a strategy developed in CFD when dealing with such wall

bounded complex turbulent flows. The wall y^+ is a non-dimensional distance defined as in equation 2-20. [21]

$$y^+ = \frac{yu_\tau}{\nu} \tag{2-20}$$

Where, y is the distance to the nearest wall,u_τ is friction velocity and ν is local kinematic viscosity of the fluid.

From fig 2-1 three zones with their corresponding y^+ wall can be observed in this viscous affected region. [21]

1. $y^+ < 5$: Viscous sublayer
2. $5 < y^+ < 30$: Blending region or buffer layer
3. $30 < y^+$: Log-law or fully turbulent region

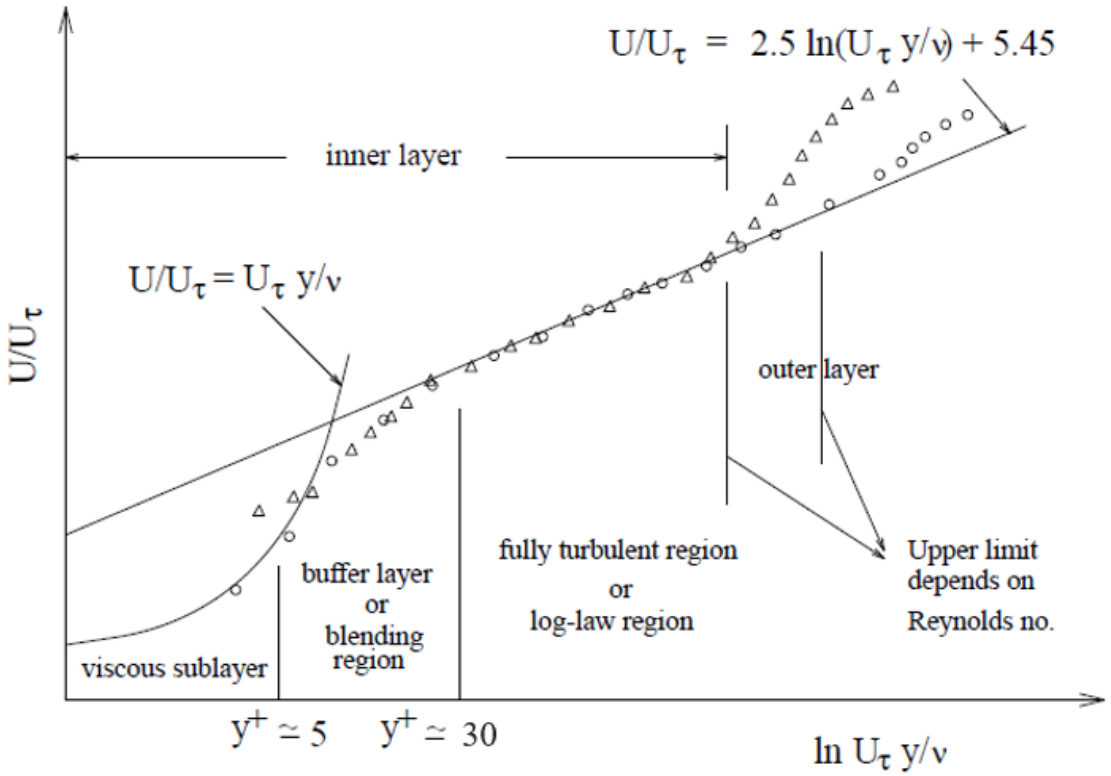

Figure 2-1: Subdivisions of near-wall region [21]

Along the viscous sublayer, the tangential velocity fluctuations are damped by the dominating viscous effects while the normal fluctuations are damped by kinematic blocking. When moved towards the outer part of near-wall region, the mean velocities have large gradients producing turbulent kinetic energy and hence an effective turbulence. As mentioned above, in order to successfully predict the wall bounded turbulent flow, it is important to accurately present

the flow in the near-wall region. Hence while mesh refining the distance of the wall to the centroid of the wall-adjacent cells is related to wall y^+ values. Values close to $y^+ = 1$ are most desired when it comes to near-wall modelling and $y^+ = 30$ when it comes to wall functions. It is advised to avoid the buffer layer while choosing the near-wall mesh size as these two functions will not accurately resolve this region.

All Wall y^+ Treatment This is a hybrid wall treatment where the model emulates the high y^+ wall treatment for coarse meshes and the low y^+ wall treatment for fine meshes. It takes results emulating with the low y^+ wall treatment as $y^+ < 5$ and with the high y^+ wall treatment as $y^+ > 30$. When it comes to meshes within intermediate resolution, i.e, all the cell-wall centroids falling under buffer region of boundary layer ($5 < y^+ < 30$) it formulates to bring out reasonable results. [22]

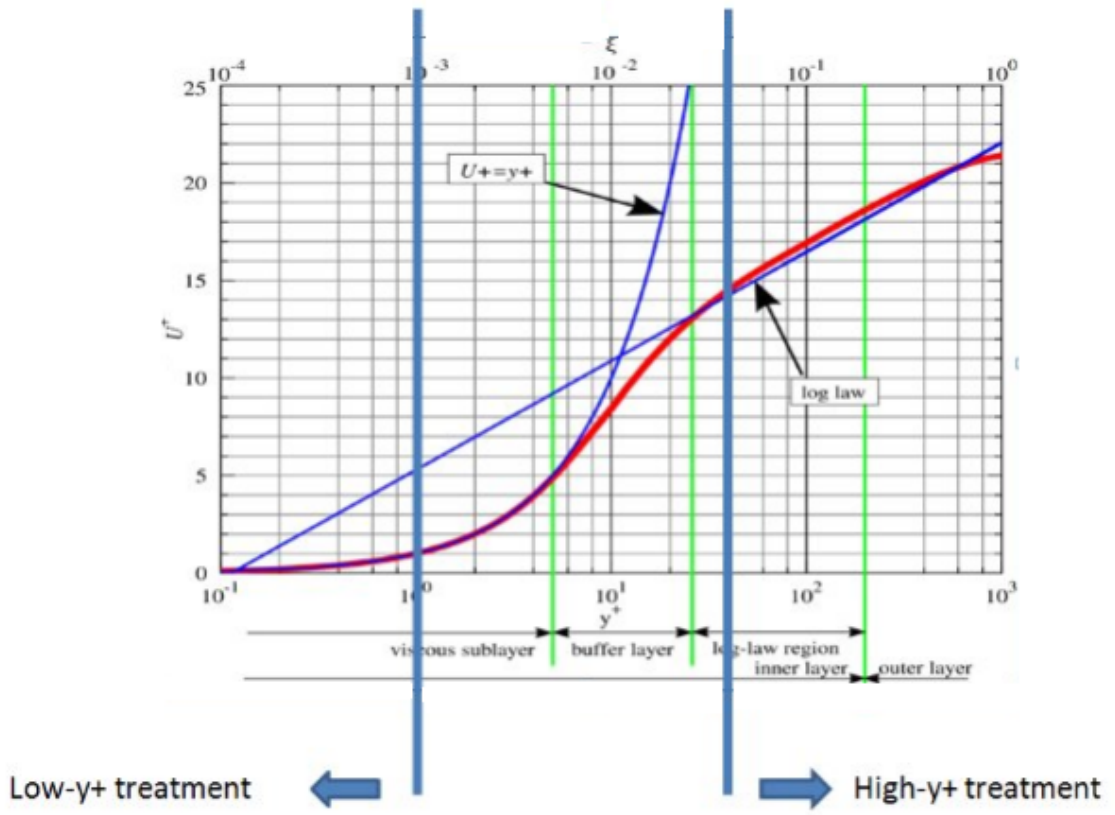

Figure 2-2: Regions of applicability of the wall treatments. [22]

In the high y^+ wall treatment approach it is assumed that the near-wall cell lies within the logarithmic region of the boundary layer. Thus the cell attached to wall will have a centroid of $y^+ > 30$. Here the equilibrium turbulent boundary layer theory is used to derive wall shear stress, turbulent dissipation and turbulent kinetic energy. The region where $y^+ < 5$ the ratio of y^+ to u^+ is approximately 1, and thus wall law is not required. For such conditions the low y^+ wall treatment approach is preferred which brings out well resolved viscous sublayer.

This hybrid method calculates turbulence quantities (TQ) such as turbulent product, stress

tensor and dissipation using an exponential weighing function, g, as shown in equation 2-21.

$$TQ = gTQ_{low\ y^+wall} + (1-g)TQ_{high\ y^+wall} \tag{2-21}$$

where,

$$g = exp\Big(-\frac{Re_y}{11}\Big) \tag{2-22}$$

and

$$Re_y = \frac{\sqrt[2]{k}y}{\nu} \tag{2-23}$$

2-2-8 Radiation Model : Surface to surface, Grey thermal radiation body

The influence of radiation in this research is significant. Hence the radiation model should provide a well refined result. The radiation is characterized in terms of radiation spectrum, spatial domain for radiation transfer solution and radiation properties. [23]

Spatial Domain for Radiation transfer solution : The radiational effects both within the region and between the regions are important in this simulation process. The model under study is in a closed set of diffuse surfaces. The Surface-to-Surface transfer model can simulate such a model. S2S model works in two steps. First step, it calculates the view factors (the proportion of surface area that the other patches illuminate) using ray tracing. The view factor is controlled by the number of patches. The view factor count is limited by the number of rays per patch with the deterministic ray tracing approach. Increase in resolution of ray tracing increases accuracy but at the cost of memory and computational time. Second step, the view factors are calculated only if there is a change in geometry and radiative properties such as spectral reflectivity and transmissivity. Thus once calculated can be reused for complex heat transfer conditions to update radiative heat fluxes from the surface temperatures. [24, 25]

An advantage of the two step approach is the computational efficiency while the disadvantage is that it often requires considerable amount of memory for storing view factors.

Radiation Spectrum : From the full electromagnetic spectrum, wavelengths ranging from 0.1 to 100 μm are pertinent to heat transfer. This thermal spectrum covers all the visible and infra-red spectrum along with a portion of the ultra-violet spectrum. A hot object emits radiation over the entire spectrum depending on the degree of hotness. Gray radiation is characterized to have radiation properties independent of wavelength of frequency. The Gray Thermal Radiation model uses the gray radiation method. Thus over the entire thermal spectrum the radiation properties are taken to be the same and over the entire thermal spectrum only a single radiative heat transfer solution is required. [11, 23]

Finally to complete the radiation model it is necessary to define the surface properties of different walls such as emissivity, reflectivity and transmissivity. Also it in necessary to define the radiative properties of the media in which it is contained as it can absorb, emit and scatter radiation.

2-3 Moving Reference Frame (MRF)

Special approaches are required while dealing with a model with static and rotating parts. Here the wheels along with the rims are considered as rotors while the remaining model is static. In such cases the flow around the moving parts appears to be steady when the observer is positioned on the rotating part. But when stationed in the static part the observer sees the same flow as unsteady in nature. This different perspective of the observer matters when one solves steady state problems unlike unsteady flow (transient) problems. Hence transferring information from stator to the rotor becomes an important issue. Changing the reference frame will affect the quantities such as acceleration, velocity and rotating tensors. [26, 27]

Use of Moving Reference Frame simplifies the transient condition to an efficient steady state case. It is a steady state approach as the fluid in the wheel rims is related to a rotating reference frame and the remaining parts of the model are related to a stationary reference frame. In other words the complete MRF defined domain is assumed to rotate at a constant angular velocity as specified, permitting the unsteady problem to become steady with respect to moving reference frame. In this approach, there is no relative velocity between the moving zone to the adjacent zone (which may be moving or stationary). The grids remain fixed during computation. It is also called frozen rotor approach as in this approach the instantaneous flow field with the rim (rotating part) in a specific position is observed similar to freezing the motion of the moving part in that position. In MRF the geometry of the rims contained in the rotating frame are considered. The rotational characteristics are directly translated at the interface between rotating and stationary regions. [28]

MRF model should be used when the flow is not complicated. As mentioned above, in this approach the rotor will always stay in the same position with respect to stator. This makes the CFD simulation highly dependent on exactly how the rotors and the stators are positioned. The MRF assumes a weak interaction between the stationary domain and rotational domain.

2-4 Volume Cell Meshers

When it comes to volume meshing after a suitable surface meshing STARCCM+ provides with different types of meshing models. Each of them have their own characteristics. In this mesh modelling few of them are considered according to their advantages over other. Since the geometry of the solids in the model is complex, choice of polyhedral meshing seemed reasonable. This is because polyhedral meshes are relatively easy and efficient to build, providing a balanced volume meshing for a given complex model. However polyhedral mesher at times find it difficult to smoothen around a region with complex geometry or with thin dimensions especially for a coarser meshing. Thin mesher becomes active at such conditions to support polyhedral mesher to complete meshing the given model accurately.

Trimmed meshers are perfect choice for larger domain. It is dominantly used for cases involving flows significantly aligned along Cartesian coordinates. Prism mesher provides cells with polyhedral base and rectangular sides. This type of cell is necessary next to wall surfaces or boundaries in order to improve the quality of the flow solutions which is critical when it comes to forces or heat transfer, flow separation etc. These two meshers are considered for meshing the fluid domain. [29]

All meshers have different advantages and disadvantages, providing with many possible combinations to select from. The meshers chosen for this model is based on the recommendation from STARCCM+ documentation and hence a detailed investigation was not undertaken over selecting these volume meshers.

Chapter 3

Reference Model

To study the influences on wind-tunnel modelling, the model of Volvo S60 is provided by the thermodynamics team, fig 3-1. The engine load case for this CFD simulation is HCTR (Hill Climbing with Trailer). Parameters and variables for this test are as follows:

- Vehicle speed : $70\frac{km}{h}$
- Air temperature : $27°C$ or $300.15K$
- Inclination : 6% increase in height over unit longitudinal distance
- Relative humidity : $< 20\%$
- Floor : Stationary

Since the parameters under investigation lies in the rear end of the vehicle, the model is split into two halves, focusing on the rear half of the vehicle. A smaller domain is defined and that will be used as the reference model for CFD simulation. This domain of dimension $3.25m \times 6m \times 0.8m$ consists of the rear half of the vehicle as shown in fig 3-1.

Solids considered in this model are split into five different parts as shown in fig 3-2. The five divisions are : exhaust system which is the heat source in this domain, heat shield, plastic shield, suspension, metal and rubber bushing and rubber (hanger). There are different thermocouple spots marked in these models in similar positions to the thermocouples used during physical tests. These thermocouple spots are referred as 'tk' in this thesis report.

The reference model consists of a final volume mesh of 14 million cells.

The boundary conditions for the reference model are taken from a previous full model CFD simulation that ran on these identical parameters, variables and engine load case, i.e HCTR. The boundaries of the reference domain are exported into NASTRAN format which are then imported to the above mentioned full model with converged solution except for the outflow

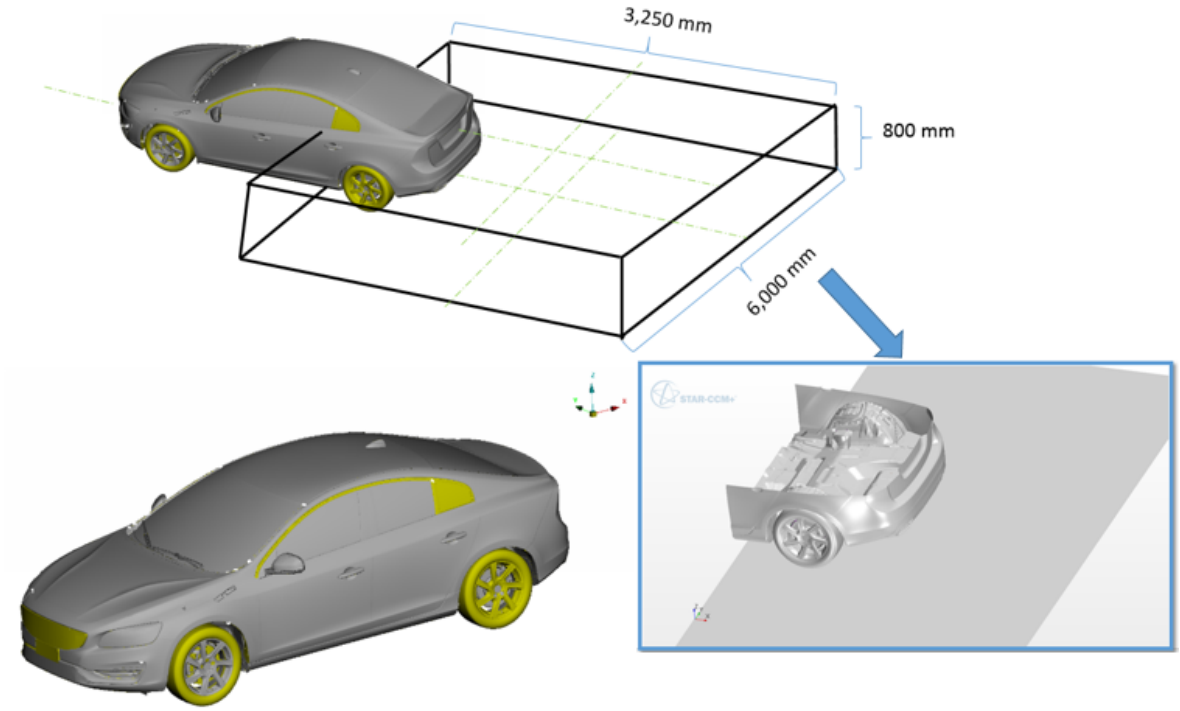

Figure 3-1: Volvo S60 CAE model and definition of domain of focus study

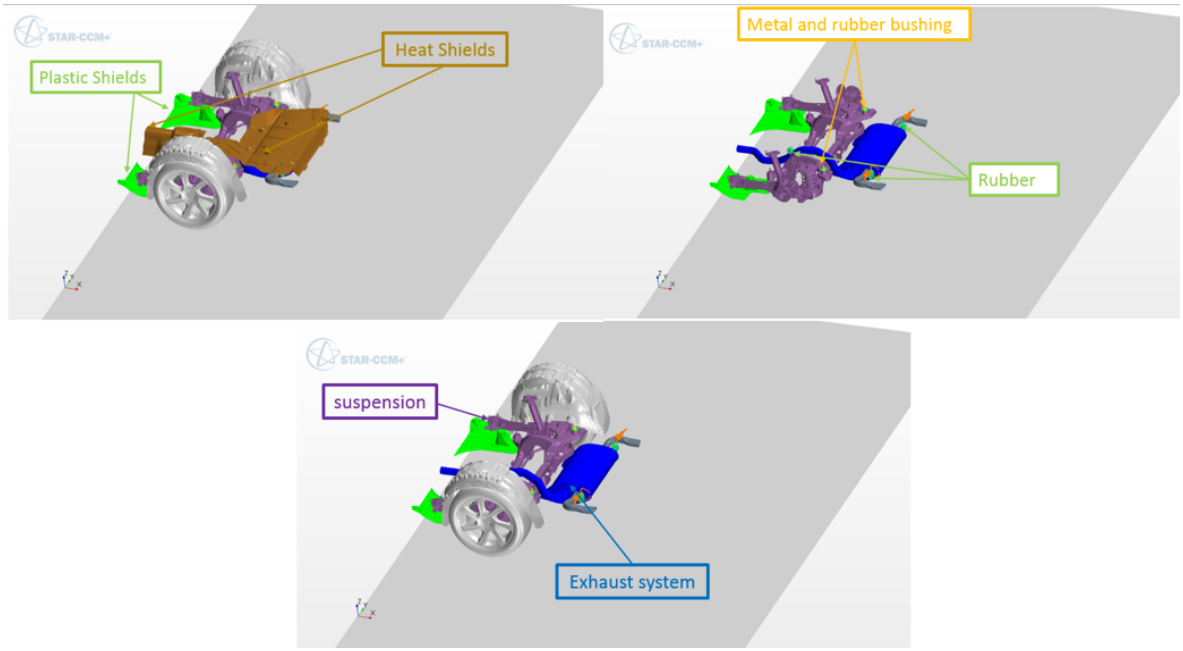

Figure 3-2: Defining the parts comprising the solids in the domain

boundary condition which is given a constant absolute total pressure of $1.1 * 10^5 Pa$. This gives an accurate positioning of the domain considered in the reference model with respect to full model. Fig 3-3 shows the domain of the reference model with respect to full model. With

the help of table extract option in STARCCM+ one can copy the values of required variables at those boundaries from the full model. In this model the values of variables copied from the full model are:

- Temperature (K)
- Turbulent dissipation rate ($\frac{m^2}{s^3}$)
- Turbulent kinetic energy ($\frac{J}{kg}$)
- Velocities in i,j,k directions ($\frac{m}{s}$)

The converged solution of the reference model simulation is judged based on the temperature plots of all thermocouple (tk) points.

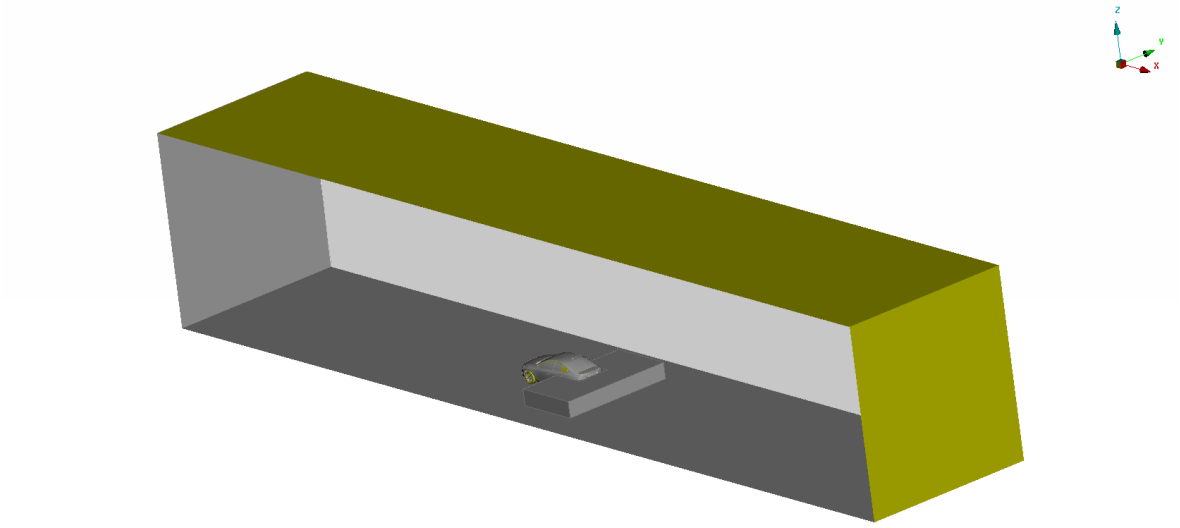

Figure 3-3: Full wind tunnel and domain of reference model

In the succeeding part of the report the comparisons of tk point readings on exhaust system and heat shield are only shown and explained. This is because the remaining divisions/ parts showed negligible temperature deviation ($< 3°C$) except the rubber. The influence over rubber depends on the positioning of tk points thus plotting for rubber isn't significant. However it is important to find the temperature gradient across the rubber. It is easy to predict the temperature gradient of the rubber depending on the surrounding metal radiations. It is found that the hind end of the rubbers located in the rear is cooled significantly due to the effective convection in these models compared to reference model.

3-1 Correlation of Reference Model over Full Model

Table in fig 3-4 shows the comparison of reference model temperature readings over full model.

The absolute temperature deviation is close to $31°C$ for exhaust system and $7°C$ for heat shield. This is acceptable for such a small domain over a relatively small number of cells compared to full model. Moreover the current study over different parameters deals with the deviation in temperature which is more important. The deviation is found to be highest around the rear part of the exhaust system. This could be due to the limitation of constant pressure outlet boundary condition, which will be explained in detail in chapter 7.

		Focused Reference Model -- Full Model *(No suction pipes in both)*
Heat Shield	tk 165	-6.12
	tk 166	0.85
	tk 167	-0.24
	tk 168	-22.42
	Absolute	7.41
Exhaust System	tk 190	11.88
	tk 191	23.99
	tk 194	25.72
	tk 221	N/A
	tk 222	N/A
	tk 269	N/A
	tk 192	11.88
	tk 193	38.58
	tk 195	56.62
	tk 196	50.45
	Absolute	31.30
		ΔT
		N/A : Data not available

Figure 3-4: Comparison of reference model temperature readings over full model

Chapter 4

Simulations of Model with Wheel Rotation and with and without MRF on Rims

In the wind tunnel the physical testing occurs with stationary rear wheels as depicted in the reference model. And when it comes to computational thermal simulation the rotation of rear wheels are considered to get closer to real road conditions. However the involvement of MRF on rims is not considered in the CFD simulation so far. Research has proven its importance in aerodynamics with its contribution on net drag and pressure distribution [30, 7, 8, 9, 31]. Its influence on pressure distribution can affect the flow underneath of the vehicle consequently affecting the convective heat transfer. However its influence on thermodynamics is seldom studied. The influence of wheel rotation and MRF on rims on the flow underneath and rear of the vehicle can be seen in the fig 4-1. The figure shows the occurrence of converging flow pattern downstream as the simulation moves from reference model to model with only wheel rotation to model with both wheel rotation and MRF on rims. The maximum convergence pattern is found for the later model.

The table shown in fig 4-2 reference the temperature deviations from the tk points. It is clear from table 4-2 that the individual influence of MRF is significant but only around specific regions. But the extent of influence due to MRF is dependent on the wheel rim profile. Also from this table the influence of these model on the heat shield is negligible except the tk 166. Hence further discussions will be focused on rear exhaust system.

4-1 Detailed Observation and Reasoning

When looked into tk 194 and tk 269, there is a decrease in temperature for both simulations (i.e, simulation with MRF on rims and wheel rotation and simulation with only wheel rotation) compared to reference simulation, fig 4-2. The wheel rotation and MRF on rims increase the average dynamic pressure of the flow under the entire rear of the vehicle making the static

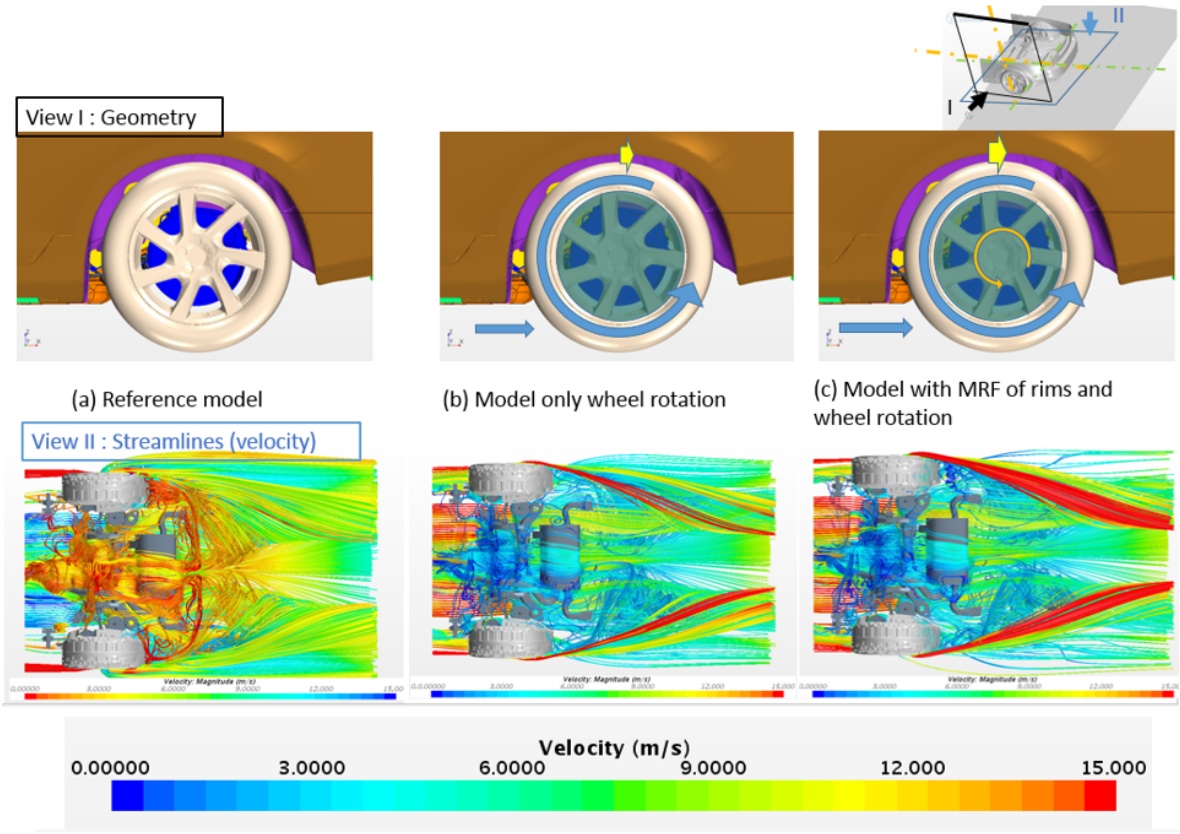

Figure 4-1: Model geometry and streamlines of reference model, model with wheel rotation and model with wheel rotation and MRF on rims

pressure more negative as shown in fig 4-3. However fig 4-4 shows that the concentration of velocity magnitude at the center of this stream disperses closer to muffler.

The flow above the upper surface of the muffler is in the upwind direction. These upwind flows are for that reason guided directly towards the on-coming downstream flow. When they meet, the vortex formed is damped and a belt of high static pressure is seen along the sides of the muffler as shown in fig 4-3. It is interesting to note that this upwind flow is in a narrow gap between the muffler and the heat shield. Therefore when the upstream flow meets the downstream flow, the vortex formed is structurally damped by the heat shield and the muffler. This makes it a more two dimensional vortex phenomena. In the reference simulation the velocity concentration of the stream flowing along the sides of the muffler damps the side-wise drift of the upwind flow coming from upper surface of muffler. The side edges of the muffler are affected the most due to the presence of two flows in opposite directions. As a consequence the vortex formed is strong and disturbs the smoother downstream flow ahead, creating more stagnant flow area along the side of the muffler. The effect of this vortex is weaker downstream flow due to the structural hindrance of the exhaust tail pipe. In the simulation with wheel rotation and MRF on rims, the static pressure is significantly low ahead of the muffler (more negative with respective to reference). This explains the larger reverse flow vortex at the side edge of the muffler. The velocity magnitude of the concentrated stream is slightly decreased resulting in a weaker and larger vortex. This enhances the flow circulation along the side

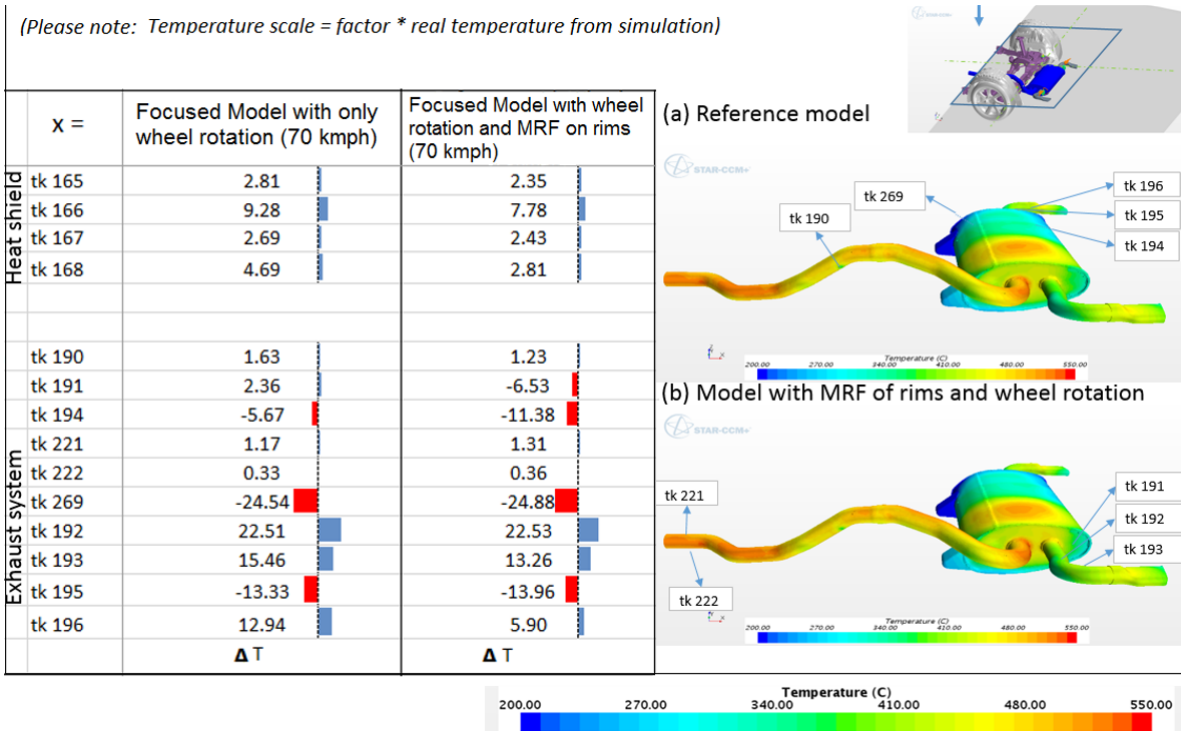

Figure 4-2: Table of temperature deviation comparison of model with only wheel rotation and model with wheel rotation and MRF on rims with respect to reference model at $70\frac{km}{h}$. The temperature deviation ΔT = Temperature reading of 'X' - Temperature reading of reference model

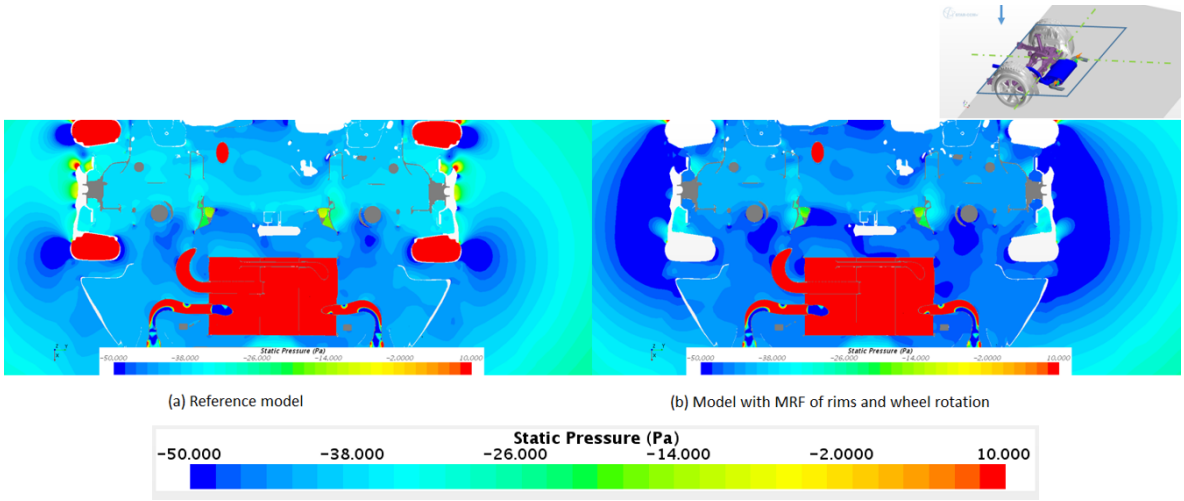

Figure 4-3: Relative static pressure comparison of reference model and model with wheel rotation and MRF on rims at tk 194 and 269 along XY axis

surface of the muffler. As a result the stagnant flow regions along the sides of the muffler are diminished. This together with better flow circulation as explained provides a better convective heat transfer along the sides of the muffler. The comparison found in fig 4-5. Fig 4-6 shows the temperature difference between the two simulations.

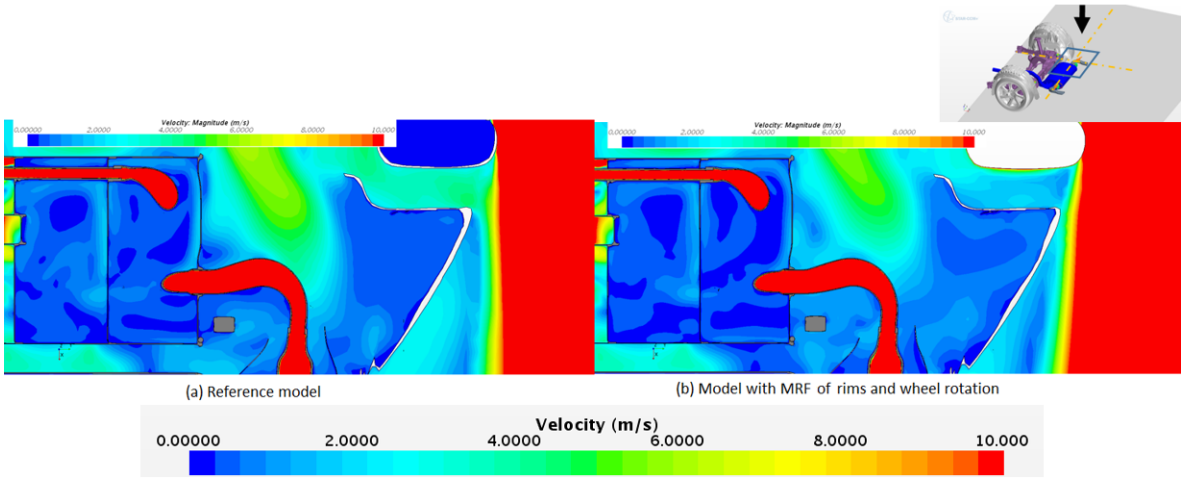

Figure 4-4: Airflow velocity comparison of reference model and model with wheel rotation and MRF on rims at tk 194 and 269 along XY axis

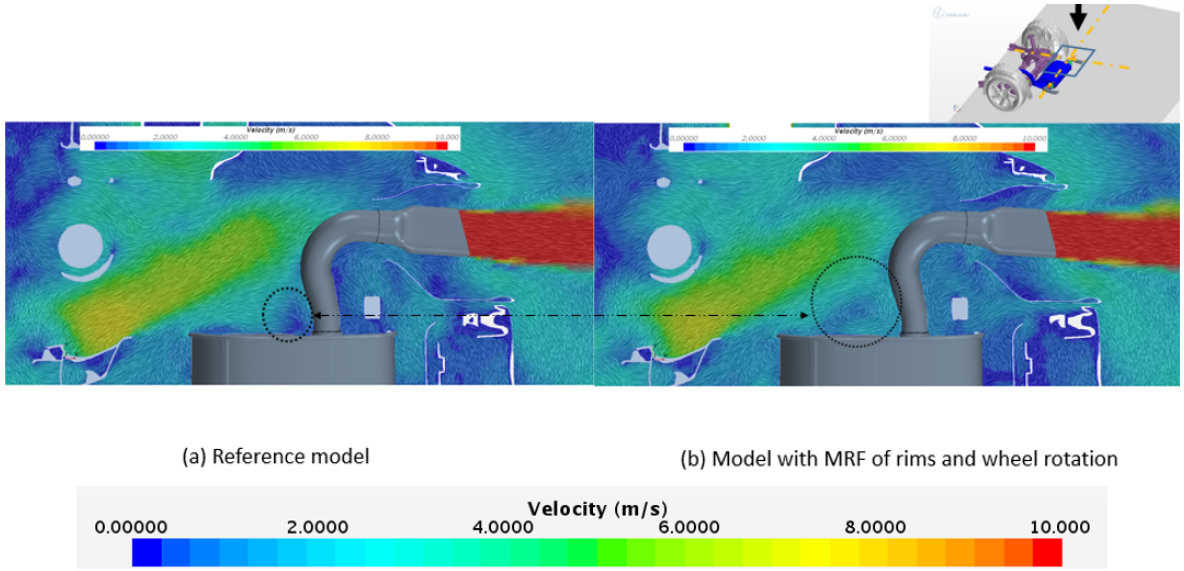

Figure 4-5: Velocity vector comparison of reference model and model with wheel rotation and MRF on rims at tk 194 and 269 along XY axis

The reason for the velocity magnitude shift is explained in the fig 4-7. When compared, a congestion around region 'A' is observed in reference simulation. Here the static pressure is high, while in simulation with MRF the congestion is minimized decreasing the static pressure. In the simulation with MRF a region between the wheel and the wheel arches, named 'B', sucks out larger quantity of air undisturbed unlike the reference case. This phenomena around 'A' and 'B' is only due to wheel rotation. This is clear when looked into the temperature difference on tk 269 as shown in table in fig 4-2. The influence of MRF on rims is dominant around tk 194. The reason is clear from the streamline patterns shown in fig 4-1. The flow is more converging to the end of the vehicle in the model with both wheel rotation and MRF on rims compared to the other two models. In other words, the mass flow rate is higher in

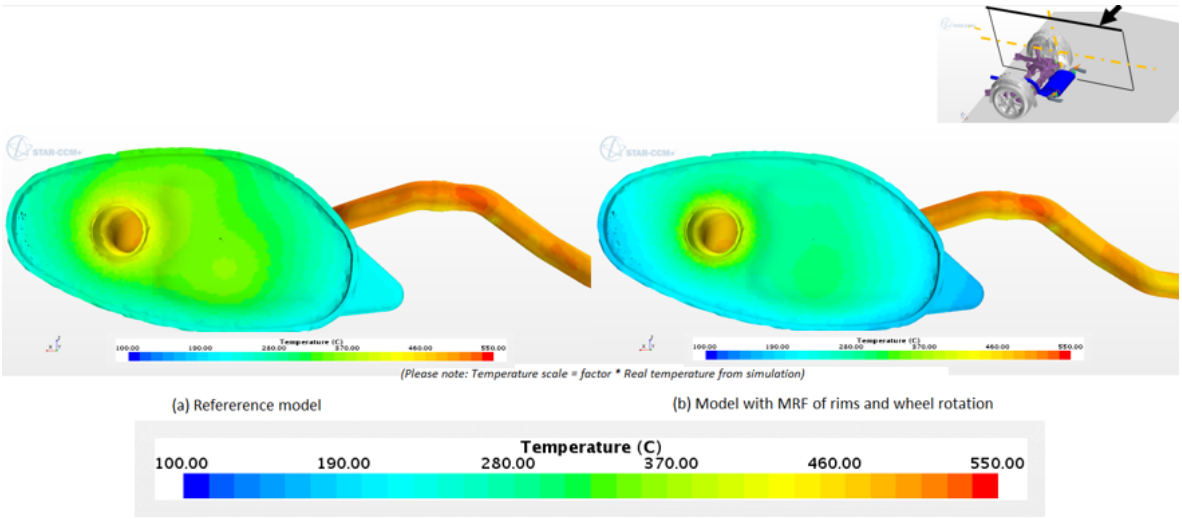

Figure 4-6: Temperature comparison of reference model and model with wheel rotation and MRF on rims at tk 194 and 269, where the temperature on scale is multiplied with a factor of exaggeration

this model compared to the other two models especially along the rear of the vehicle resulting in a more effective convective heat transfer. Similar is the case for tk 191. The temperature difference (i.e, decrease in temperature) has doubled in simulation with both MRF on rims and wheel rotation compared to one with only wheel rotation, table 4-2.

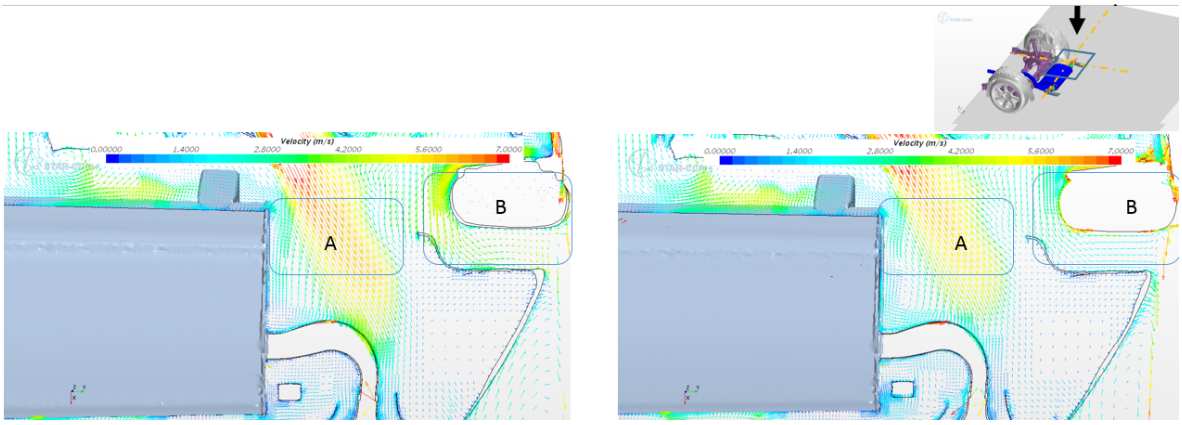

Figure 4-7: Airflow comparison of reference model and model with wheel rotation and MRF on rims over the regions 'A' and 'B' along XY axis

On tk 192 and 193, as seen in the table in fig 4-2 the readings around these regions show increase in temperature. When considering the region downstream close to exhaust tail pipe, i.e, regions that cover tk 192 and 193, the velocities are higher in reference condition than one with MRF on rims and wheel rotation or one with only wheel rotation. However the decrease in velocity is insignificant when compared to increase in temperature (avg. 18 degree Celsius). This rules out the influence of decrease in velocity rate. Here the direction of flow provides the key to the reasoning. Fig 4-8 and 4-9 show the flow of hot air downstream after cooling

the upstream solids with high temperatures in both cases. A fraction of this air gets collected in the voids between under-body and rear of exterior heating the region surrounding the void, while remaining washes out downstream. However in the case with MRF these hot air gets concentrated into a steady vortex close to the region sandwiched between the exhaust inlet pipe to the muffler and exhaust outlet pipe from the muffler. This creates a hot zone around this region. The vortex formed sucks in the hot air downstream that flowed between muffler and heat shield. Hence the temperature of air surrounding this region is high. This decreases the temperature difference between the adjacent solids and air thus decreasing the convective heat transfer as clearly shown with equation 2-2. It is shown in fig 4-10 where the conduction in simulation with MRF is reduced due to the decrease in temperature difference. This explains the higher temperature along the surface facing upwind of the exhaust tail pipe consisting of tk 192 and 193. As a result inefficient convection and high conduction from this region explains the raise in temperature on tk 192.

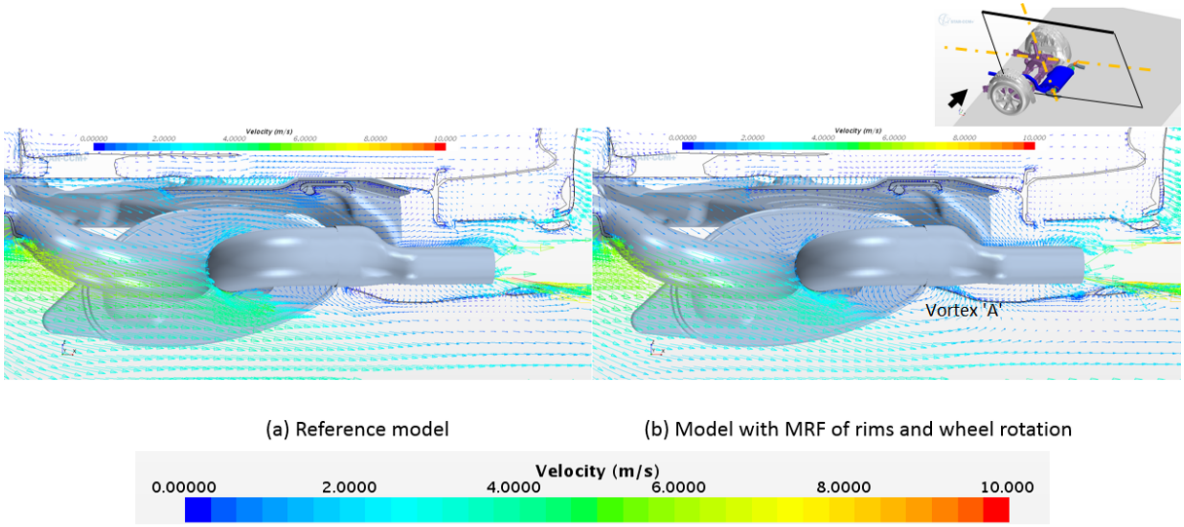

Figure 4-8: Airflow velocity comparison of reference model and model with wheel rotation and MRF on rims at tk 192 and 193 along XZ axis

Moreover, unlike the reference case, in simulation with MRF two new vortices are generated just below the exhaust tail pipe close to region surrounding tk 193. They re-circulate hot air in this region similar to the above case hence reducing the temperature gradient between the exhaust pipe wall and air surrounding it, resulting in a reduced convective heat transfer. From fig 4-8 the vortex direction 'A' is visible. The vortex from the point of view is counter clockwise opposing the flow downstream. This explains the average reduction in velocity magnitude in the case with MRF.

Fig 4-3 shows the influence of the lower static pressure ahead of the sleeve. Due to lower static pressure ahead the air close to exhaust tail pipe outlet (i.e, surrounding the sleeve) moves inwards taking part in recirculation resulting in forming the vortex close to tk 193 as shown in fig 4-11. In addition this inward air flow is heated up by the exhaust tail pipe on the way to tk 193 decreasing the temperature gradient between the solid and air surrounding the region tk 193.

The temperature reading at tk 195 is lower in simulation with MRF compared to the reference

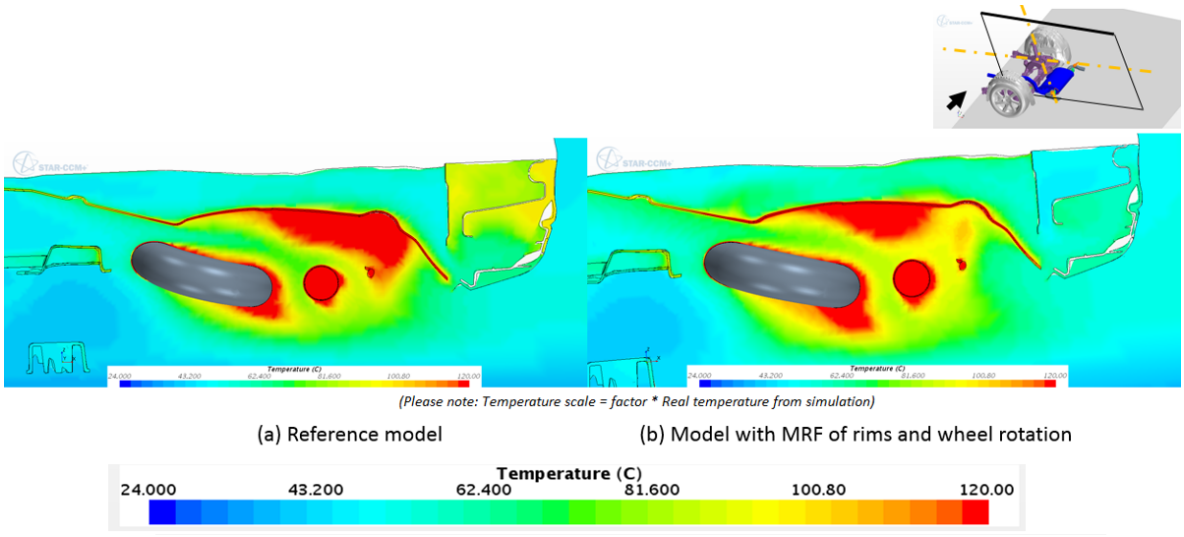

Figure 4-9: Comparison of air temperature of reference model and model with wheel rotation and MRF on rims over the regions of tk 192 and 193 along XZ axis, where the temperature on scale is multiplied with a factor of exaggeration

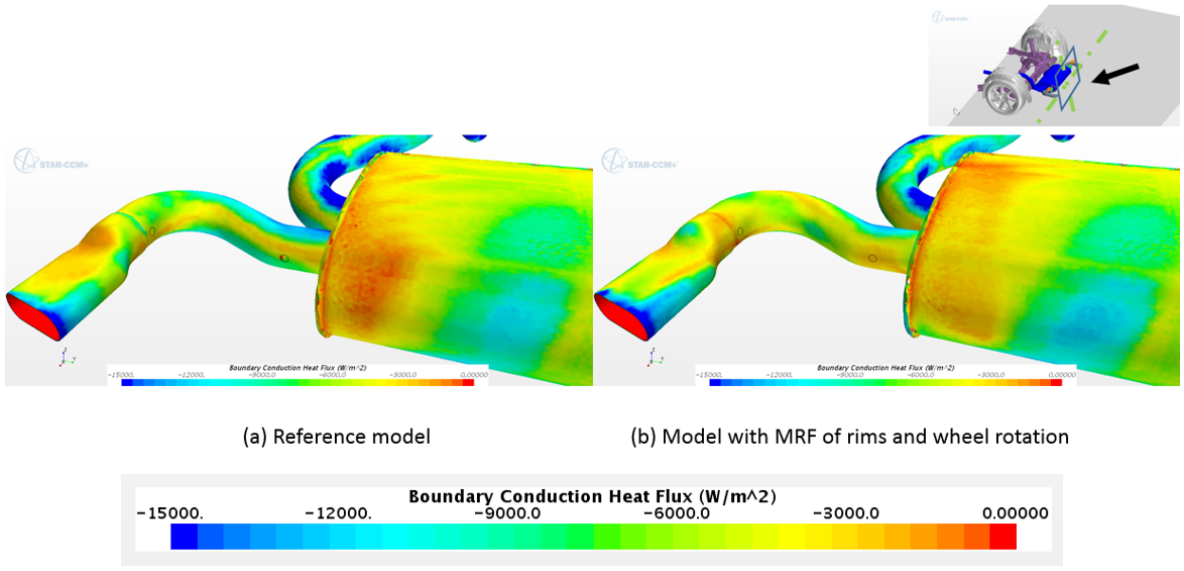

Figure 4-10: Comparison of convective heat transfer of reference model and model with wheel rotation and MRF on rims over the regions of tk 192 and 193

simulation. Even though tk 195 is placed in similar position as tk 192 in the opposite exhaust tail pipe, the temperature deviation is in the opposite direction. This is because firstly, they are not placed symmetrically in terms of coordinates. Tk 195 is close to muffler by 25 mm while tk 192 is closer to muffler by 66 mm. Secondly, unlike tk 192 there is no presence of exhaust pipe inlet to the muffler in front of the respective tail pipe. Since this exhaust tail pipe is considered as the heat source of the simulation, position of the same has a significant influence. Therefore the flow around the region consisting of tk 195 is cooler. This increase in temperature difference enhances convective heat transfer. The hot zone, as explained in

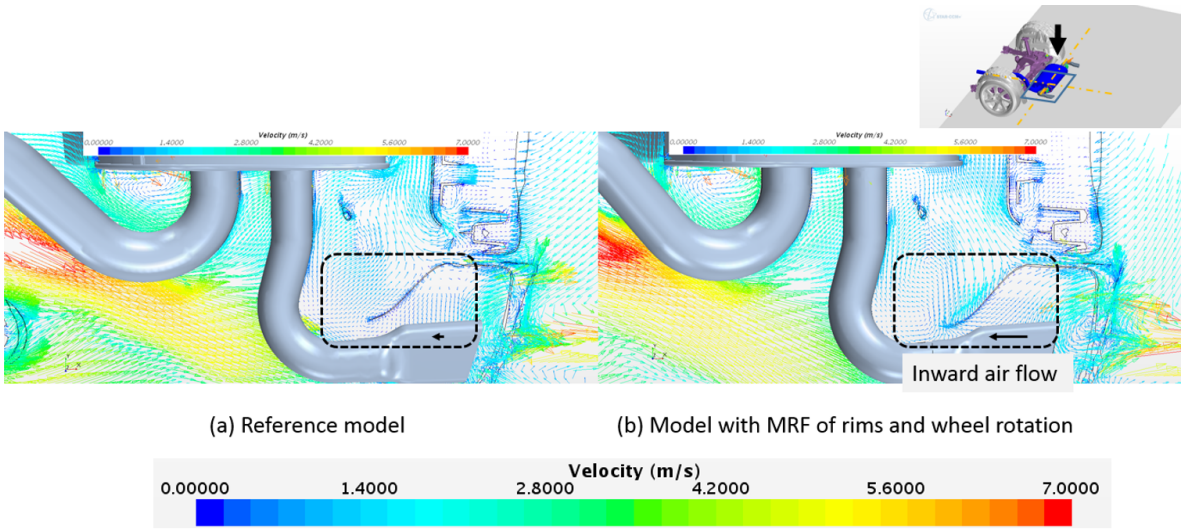

Figure 4-11: Velocity vector comparison of reference model and model with wheel rotation and MRF on rims at tk 192 and 193 along XY axis, explaining the upstream flow through the sleeves

the temperature deviation of tk 192, differentiates the trend one expects from tk 195 in comparison to tk 192.

Finally, the exhaust rear muffler is not placed symmetrically. As a result, one side is closer to the wheel compared to other. The side consisting of tk 269, 194, 195 and 196 is shifted closer to the wheel in comparison to the side consisting of tk 191, 192 and 193. As a consequence, the influence of wheel rotation and MRF is more predominant on the side closer to the wheel. Checking the radiation and convection over the total heat flux in these regions as shown in fig 4-12, shows the dominance of convection. Any change in total heat flux in the simulation with MRF is due to the effective convection. In this condition the temperature of exhaust gases are not affected and hence remain same as reference case. The variation of radiation is only a side effect of effective convection.

The region of tk 196 the hot air that absorbs the heat from the top and front surface of the exhaust tail pipe flows around the back of the same pipe. In reference model the flow is undisturbed while in the simulation with MRF the presence of an up-wash creates a stagnant region. So the heat transfer in this region becomes difficult. This is visible from fig 4-12 showing the difference in convection for the two cases.

4-2 Conclusion

The influence of wheel rotation and MRF on rims is quantified. The influence of wheel rotation is more dominant when compared to that of MRF on rims. Though MRF on wheels influence only certain regions, the magnitude of the influence is notable (approximately double that of model without MRF on rims). The table in fig 4-2 compares the two parameters and the influence of the individual is vivid. The important point to remember in this conclusion is that the influence of wheel rotation will remain same in general for the given wheel diameter, tyre thread profile and ride height. But the the influence of the MRF on rims is only quantified

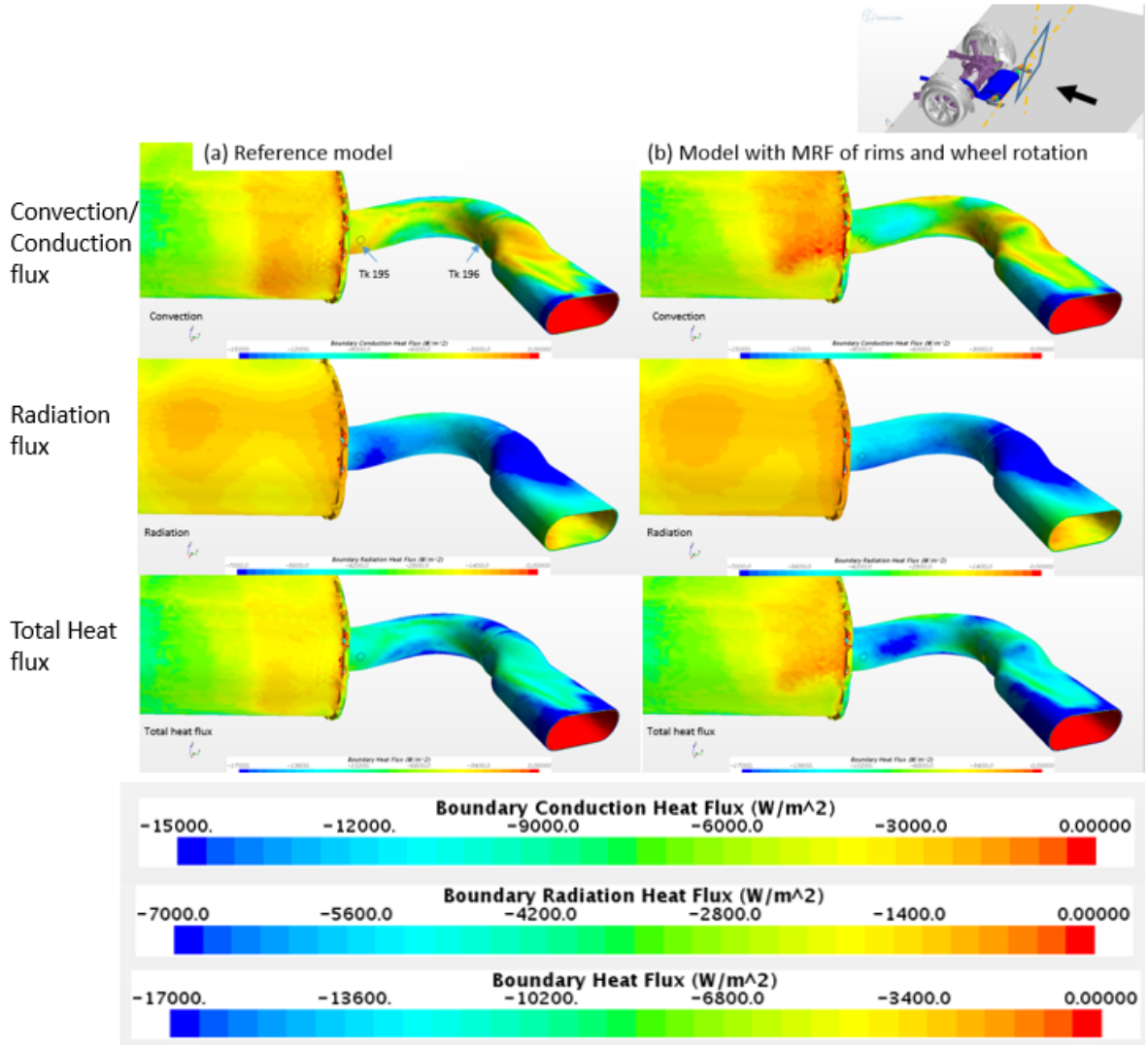

Figure 4-12: Comparison of Heat transfer of reference model and model with wheel rotation and MRF on rims over the regions of tk 195 and 196, showing dominance of convection

for a given custom rim profile and its influence for different rim profiles cannot be concluded with a single solution. This is because this rim profile gave more or less a suck-in effect to the air that entered from the outer sides of the wheel. If the profile given provides a more effective suck-in/suck-out effect the results obtained will be different. Since the under-body is a complex geometry a general conclusion for the influence of MRF cannot be deduced and its extent of influence is based on the given rim profile. In addition it is also noticeable that the temperature deviation is almost similar around the tk points 221, 222 and 190, which implies that there is no influence of this parameter upstream. Hence only the rear part of the vehicle has any noticeable influence due to these parameters. As mentioned in section 2-3 the MRF method is a steady state approach and it observes an instantaneous flow field with the rim (rotating part) in a specific position. Sliding mesh technique can be used for a more detailed study as it uses transient condition which is more realistic in nature. However the time consumed for this transient approach is too high.

Chapter 5

Simulation of Model with Exhaust Suction Pipes

The test section of the wind tunnel at Volvo cars is split into two. The front half is where the aerodynamics team conduct their tests while the second half is for the thermodynamics team. As mentioned in section 1-2 during the test they attach exhaust suction pipes to absorb all the emissions coming out of the exhaust system hence preventing it from being released into the wind tunnel chamber as shown in fig 5-1. Mass flow rate of air being drawn by these suction pipes is the best possible boundary condition that can be deduced from the given provisions. In order to calculate the mass flow rate of suction various velocity readings of air were taken at the mouth of the pipe using anemometer with different blockages at the mouth of the pipe as shown in fig 5-2. These experimental values were then taken as input for a separate the exhaust suction pipe simulation providing an average mass flow rate. This mass flow rate is then taken as the boundary condition at the suction pipe inlet for this CFD simulation model.

The table shown in fig 5-3 shows the influence of exhaust suction pipes on the vehicle's thermal results. The trend of temperature is to decrease compared to reference simulation as shown in this table. This phenomena is due to the decrease in pressure inside the muffler, especially in the exhaust inlet chamber, sketched in fig 5-4. In the reference model there is a pressure gradient across the three chambers resulting in an effective flow circulation and thus a smoother heat transfer from one chamber to another. When it comes to the model with exhaust suction pipes this pressure gradient is negligible hence there isn't any effective flow circulation or air movement from one chamber to another. This dampens the heat transfer across the chambers as mentioned in detail in the next section.

5-1 Detailed Observation and Reasoning

Exhaust System : The temperature deviation at tk 191 is positive. This implies that the temperature at this point is higher in the model with exhaust suction pipes compared to the

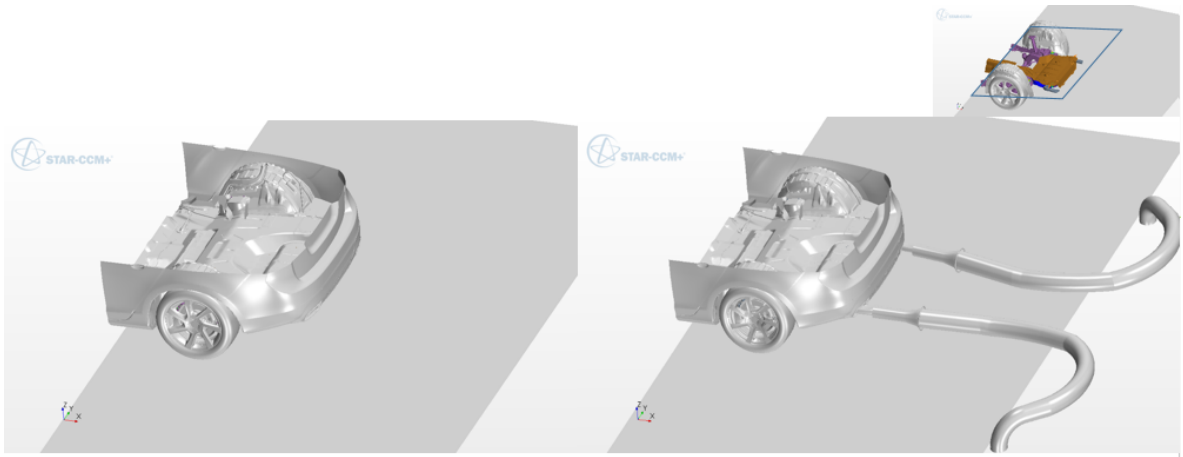

(a) Reference model (b) Model with exhaust suction pipe

Figure 5-1: Model geometry of reference model and model with exhaust suction pipes

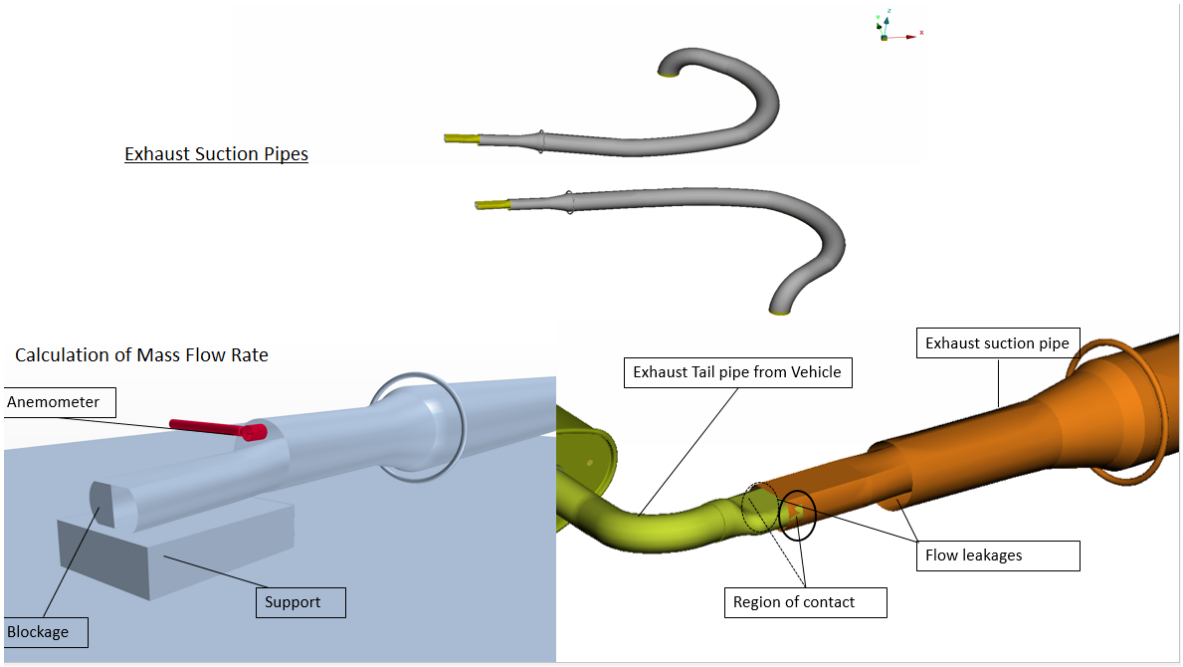

Figure 5-2: Figure showing the experimental reading and the junction connecting the exhaust tail pipe and suction pipe

reference model. The fig 5-5 shows the flow of exhaust gas inside the muffler. In reference model the flow along the region close to tk 191 is stagnant reducing the heat transfer from hotter air to the wall with tk 191. In model with exhaust suction this stagnation region shifts upwards. This improves convection in the inner wall of the muffler heating tk 191. Hence the increase in temperature in this region is just a local phenomena. In general the trend of temperature is to decrease when a suction pipes is attached. Through further investigation fig 5-6 shows the convection between exhaust gas and inner wall of the muffler. (Keep in

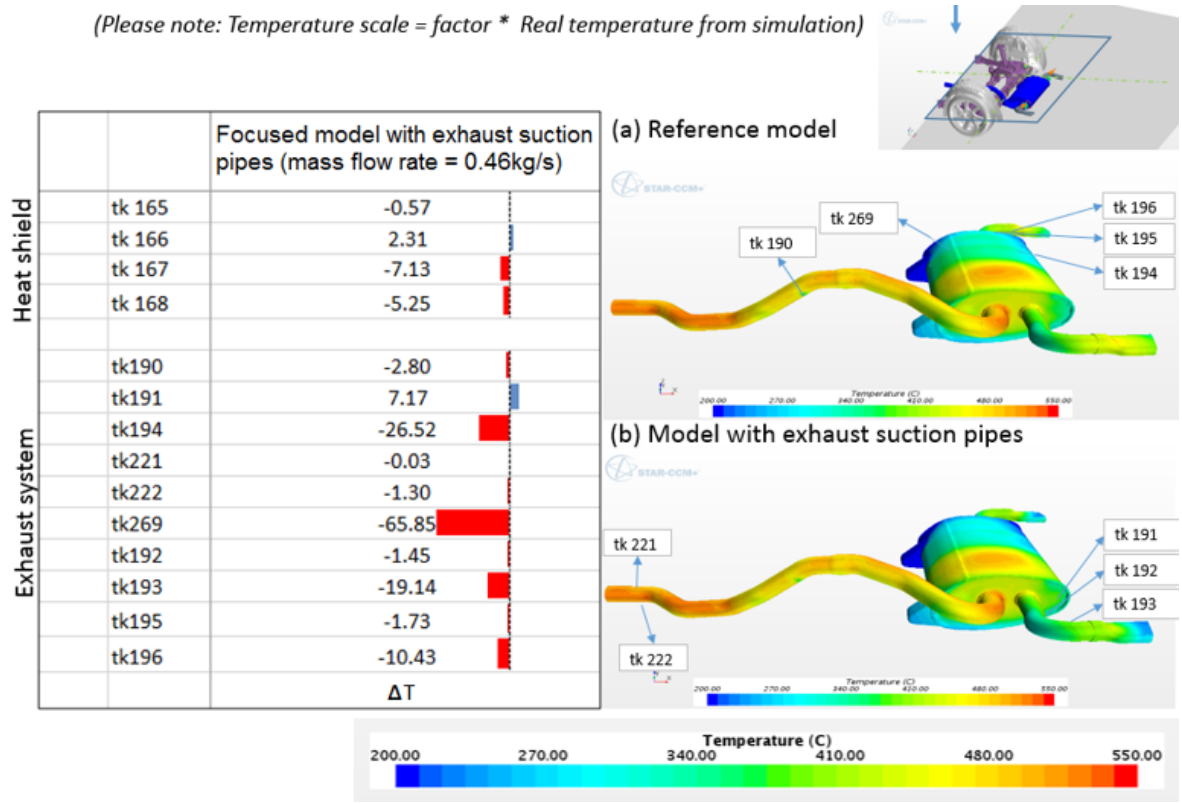

Figure 5-3: Table of temperature deviation between reference model and model with exhaust suction pipes at vehicle velocity $= 70\frac{km}{h}$. The temperature deviation, ΔT = Temperature reading of model with exhaust suction pipes - Temperature reading of reference model

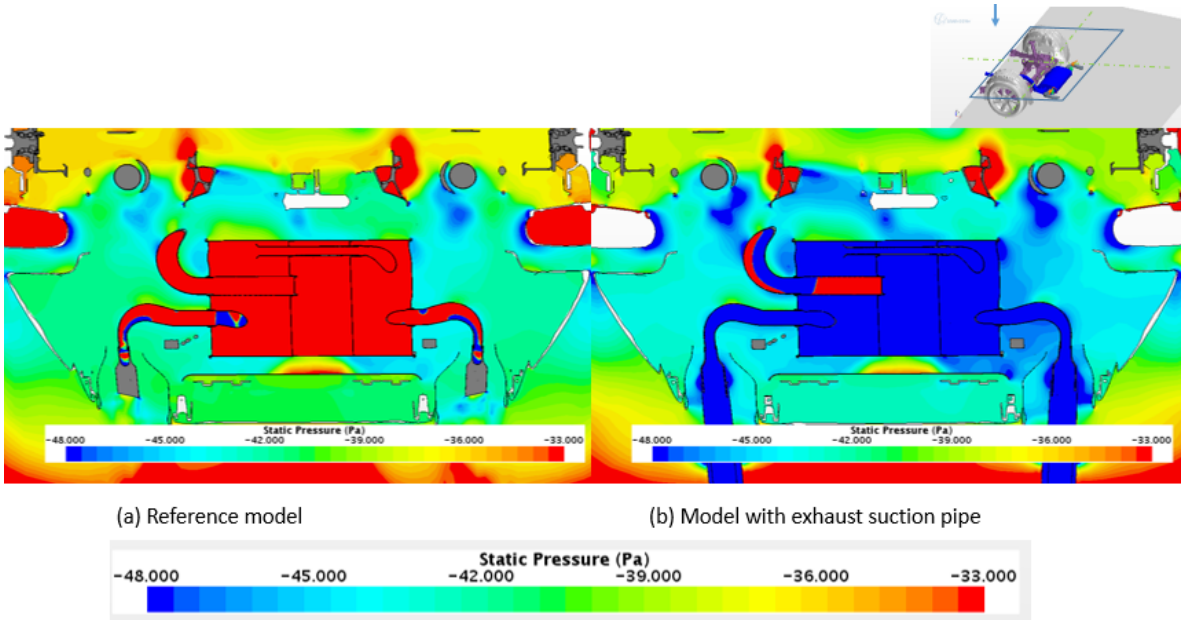

Figure 5-4: Pressure comparison between reference model and model with exhaust suction pipes

mind that negative in scale, i.e, towards dark blue shows that the heat is transferred out from exhaust gas to inner wall of the muffler). Fig 5-6 shows light blue colour around the specific region surrounding tk 191 which explains the inefficiency of the heat transfer due to poor inner flow around the corners. Comparison in the fig 5-6 (a) and (b) shows the upper shift of this stagnation. This local phenomena is not reliable because of two possible reasons. Firstly, the flow model used is for steady state condition while the flow inside is complex and possibly of transient characteristics, locally around tk 191 inside the muffler that could fluctuate this regional flow stagnation up and down providing a logical reason to this observation. Secondly, the volume mesh pattern formed by the mesher inside the exhaust muffler between the two models are not identical hence effecting the flow pattern in micro level.

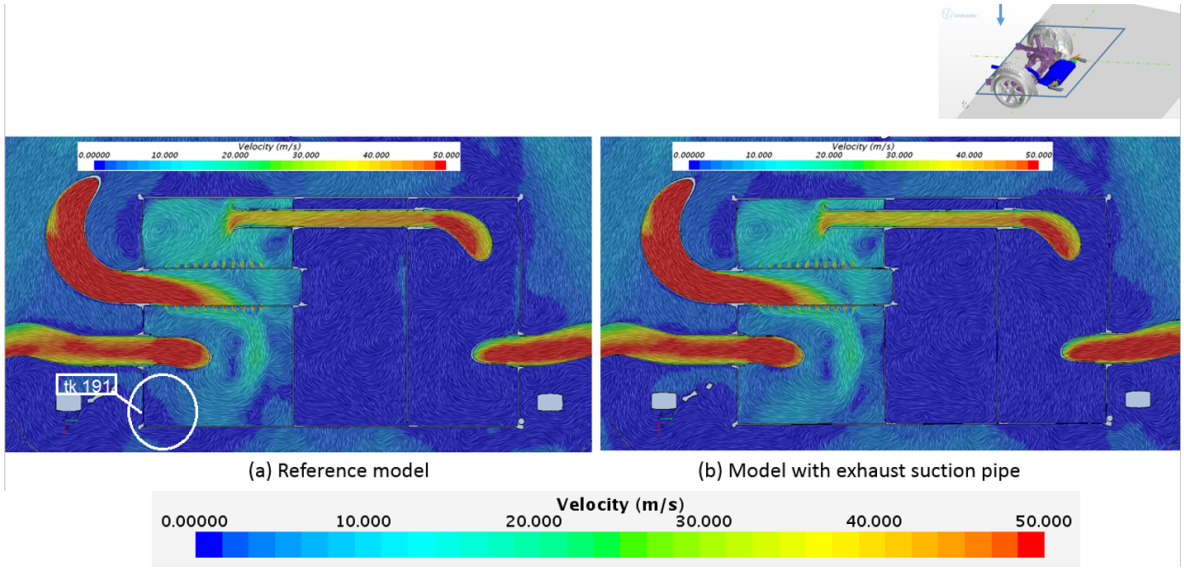

Figure 5-5: Velocity comparison of exhaust system between reference model and model with exhaust suction pipes at tk 191,194 and 269 along XY plane

The temperature deviation is negative at both tk 269 and tk 194. This implies that the temperatures have decreased around this region for this model in comparison to reference model. In fig 5-7-(a) showing the convection heat transfer on the inner wall of the muffler consisting of tk 269 and tk 194 highlights a dark blue region of concentrated heat transfer. When cross-sectioned through this region one finds the location of the connecting pipes that connects this chamber 'C' to the main chamber 'A' as shown in the fig 5-8. However in the model with exhaust suction pipes, this dark blue region is absent, fig 5-7-(b). The reason for such a blue region of concentrated heat transfer lies on the velocity magnitude through the connecting pipes that connect these chambers. This is because, in steady state the circulation between the chambers are high in reference case due to the presence of high pressure exhaust gas from the exhaust pipes inlet to the muffler. Since the outlet of the tail pipes is at pressure close to atmospheric pressure, the pressure in general is higher inside the muffler with increase in pressure at the main chamber, i.e, 'A'. Presence of such high local pressure gradient increases the magnitude of flow circulation velocity between the chambers. This movement of mass flow provides an effective heat transfer though the chambers. As a result the mass flow through connecting pipes transfer significant amount of heat in the form of convection as shown in by the dark blue region of concentrated heat transfer. In the case with exhaust suction pipes

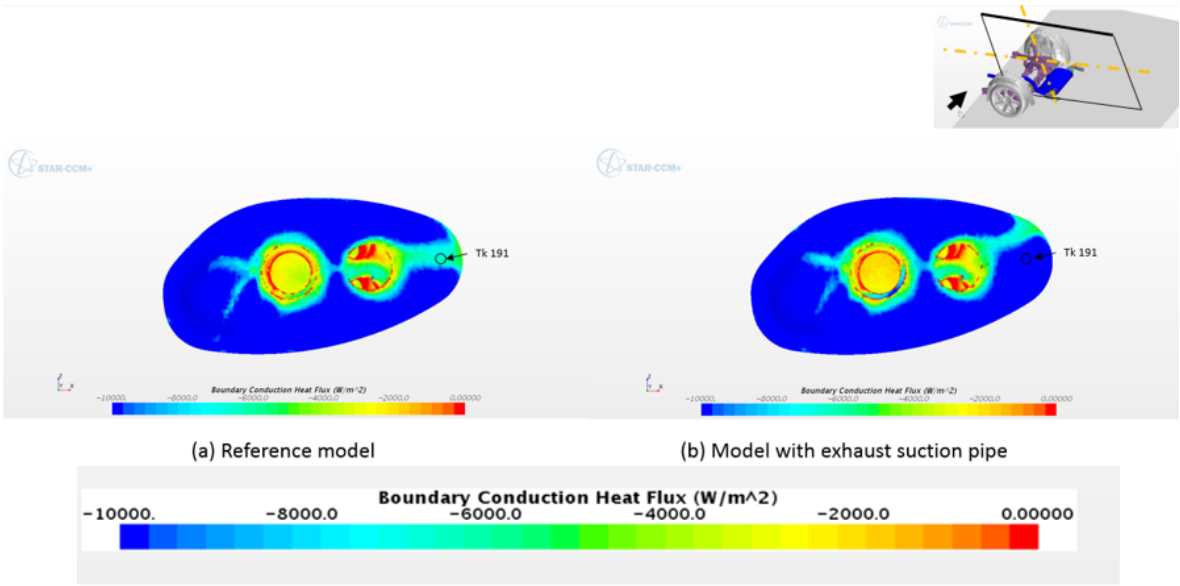

Figure 5-6: Inner surface convection comparison of exhaust system between reference model and model with exhaust suction pipes at tk 191 along XZ plane

which are attached at the end of tail pipes outlet the pressure inside the muffler reduces to a lower pressure than atmospheric pressure and the pressure gradient across the chambers are very low. This causes the steady circulation velocity to reduce significantly, even closer to zero in average across the connecting pipes. This reduction in mass flow affects the heat transfer from chamber 'A' to chamber 'B'. This is visible when looking at the velocity through the plane cutting through the pipes connecting the chambers as shown in fig 5-8 and also supported by the streamline pattern inside the muffler 5-9.

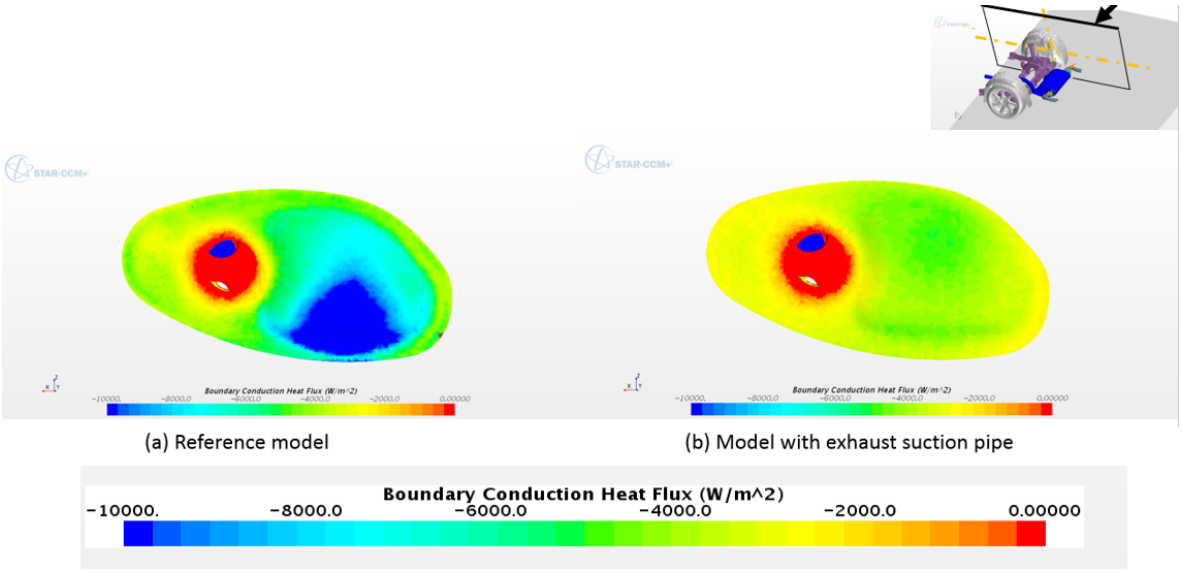

Figure 5-7: Inner surface convection comparison of exhaust system between reference model and model with exhaust suction pipes at tk 194 and 269 along XZ plane

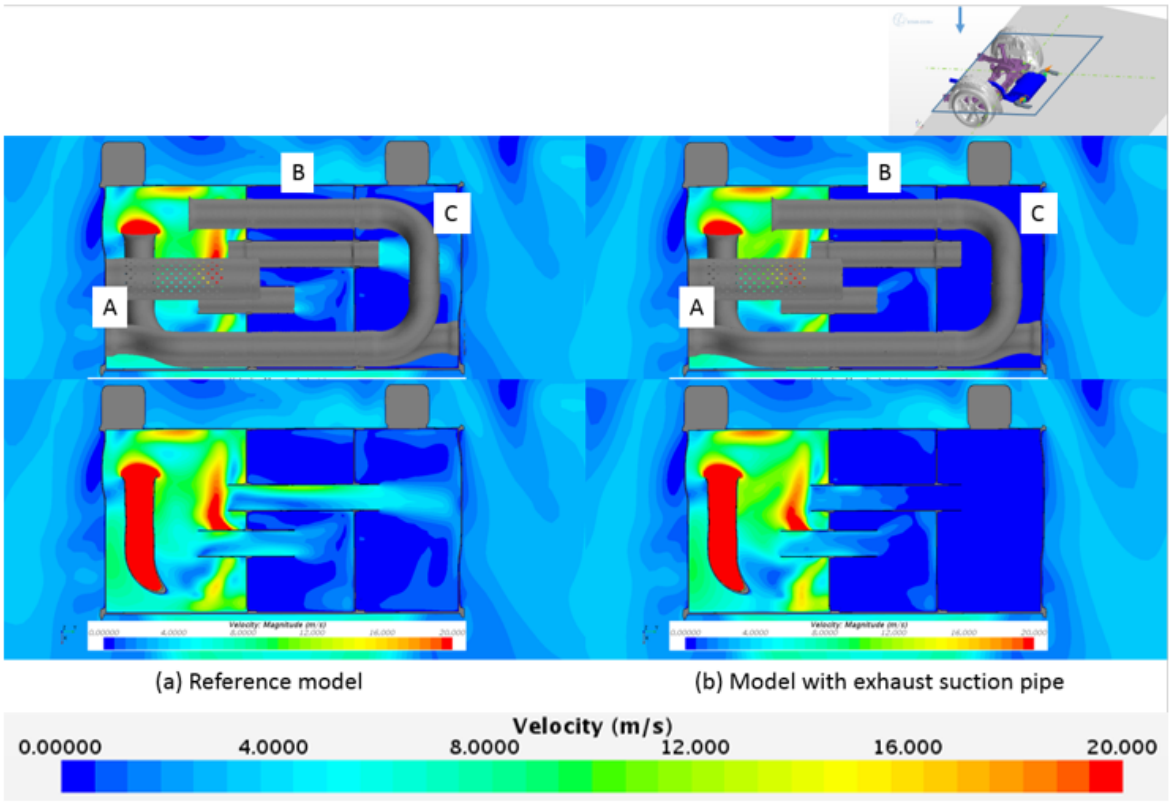

Figure 5-8: Velocity comparison of exhaust system between reference model and model with exhaust suction pipes at tk 194 and 269 along XY plane

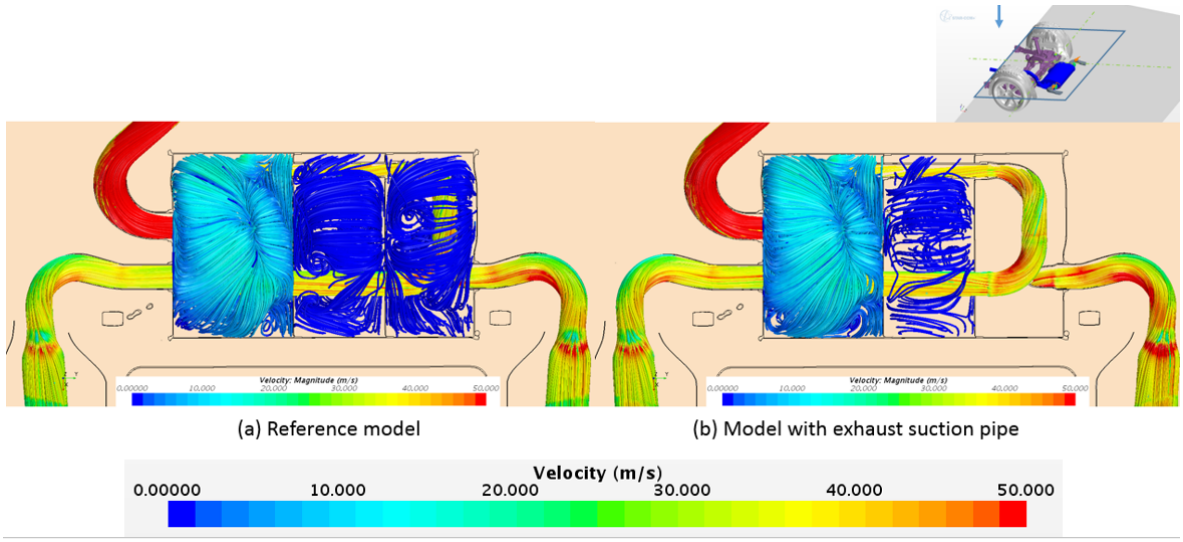

Figure 5-9: Comparison of streamlines inside muffler of exhaust system between reference model and model with exhaust suction pipes at tk 194 and 269 along XY plane

It is seen that the ambient air temperature underneath the vehicle of the reference model, shown in fig 5-10, is high. This is due to the fact that certain amount of air remains locked

in the rear after cooling the muffler and heat shield. This air takes heat from heat sources, i.e exhaust system, and then raise the average heat of air that flows underneath the vehicle. This is due to the complex exterior wall geometry (here only the rear bumper is considered) of the vehicle. This wall has sealed the air from directly flowing to the ambient air behind the vehicle, as a result this hot air recirculates.This unnecessary recirculation heats up the flow underneath the vehicle and the average heat of air in this region increases reducing the convection heat transfer (reduced temperature gradient). Also the presence of these re-circulations disturbs the smooth flow underneath the vehicle. As mentioned previously the exhaust suction pipes have leakages directly close to the exhaust tail pipes. When the exhaust suction pipes are implemented all these recirculating hot air is drawn out from underneath the vehicle. This adds provision for cooler air to flow underneath the vehicle as shown in fig 5-10. In addition this suction increases the velocity magnitude of air flowing underneath, enhancing the convection. The presence of complex under-body geometry blockages minimize this effect to regions close to the suction such as areas around tk 193 and 196. Fig 5-11 depict this effect. The suction effect of the exhaust suction pipes also has intensified convective heat transfer between the exhaust gas and the exhaust tail pipes' inner walls. As shown in fig 5-12 the regions along the end of the tail pipes have transferred appreciable amount of heat through effective convection due to the increased mass flow rate by the exhaust suction pipes. The temperature at these regions are very low (close to ambient air temperature). The presence of such high temperature gradient promotes high conduction throughout the exhaust tail pipes.

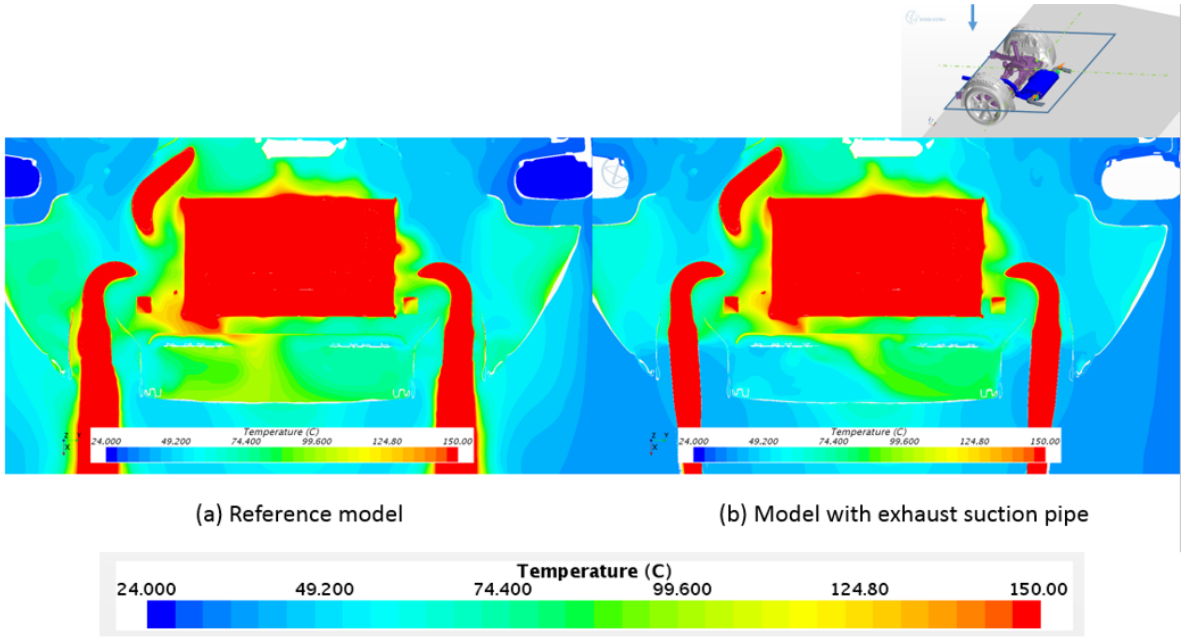

Figure 5-10: Comparison of air temperature surrounding exhaust system between reference model and model with exhaust suction pipes at tk 193 and 196 along XY plane

Such an explanation can be used in the case of tk 193 but for tk 196 there is an exception over local inner wall convection in the region covering tk 196. When considering tk 196 the local conduction in the outer region, i.e between outer wall of the exhaust tail pipe and air flowing outside, is lower compared to the reference model. When looking into the inner wall convection, it is seen that the local convection between exhaust gas inside and inner wall close

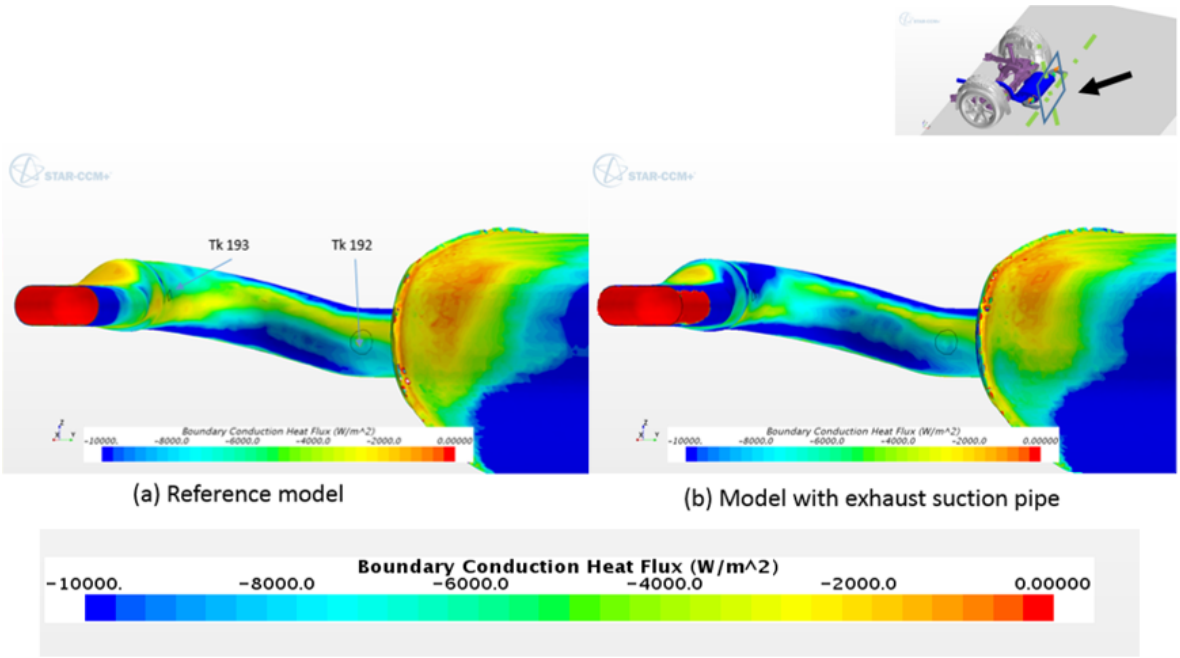

Figure 5-11: Convection comparison of exhaust system between reference model and model with exhaust suction pipes at tk 192 and 193

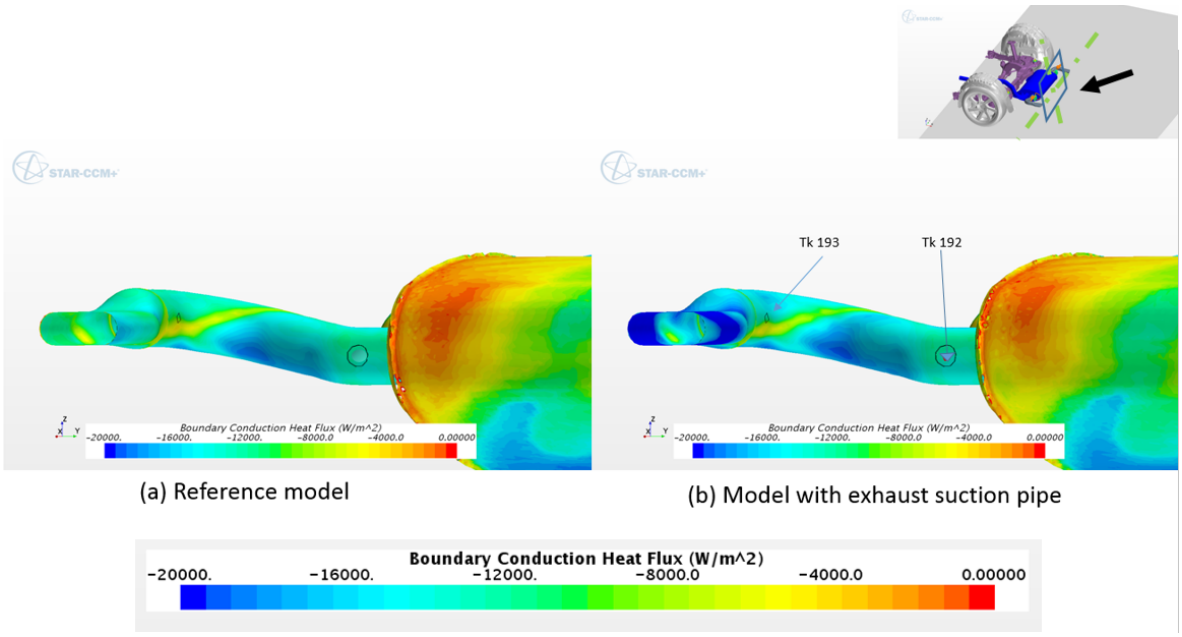

Figure 5-12: Inner surface convection comparison of exhaust system between reference model and model with exhaust suction pipes at tk 192 and 193

to tk 196 is higher than reference model. The fig 5-13 and 5-14 show the above mentioned occurrence. This should increase the temperature locally at tk 196 but in final comparison the temperature reading shows a decrease in temperature at tk 196 for simulation of model with exhaust suction pipes when compared to reference model simulation. This is due to the

dominance of conductive heat transfer. The increase in temperature is concentrated to only a very small region while the dominance of conduction is appreciably high contributing to net decrease in temperature for the simulation of model with exhaust suction. The reduction of local convection in the outer wall of tk 196 is due to the stagnation of the flow. Although it is only in a small region where its influence is notable as mentioned above. This flow behaviour is due to the unsymmetrical placement of rear muffler. In tk 193 the temperature decrease is higher than tk 196.

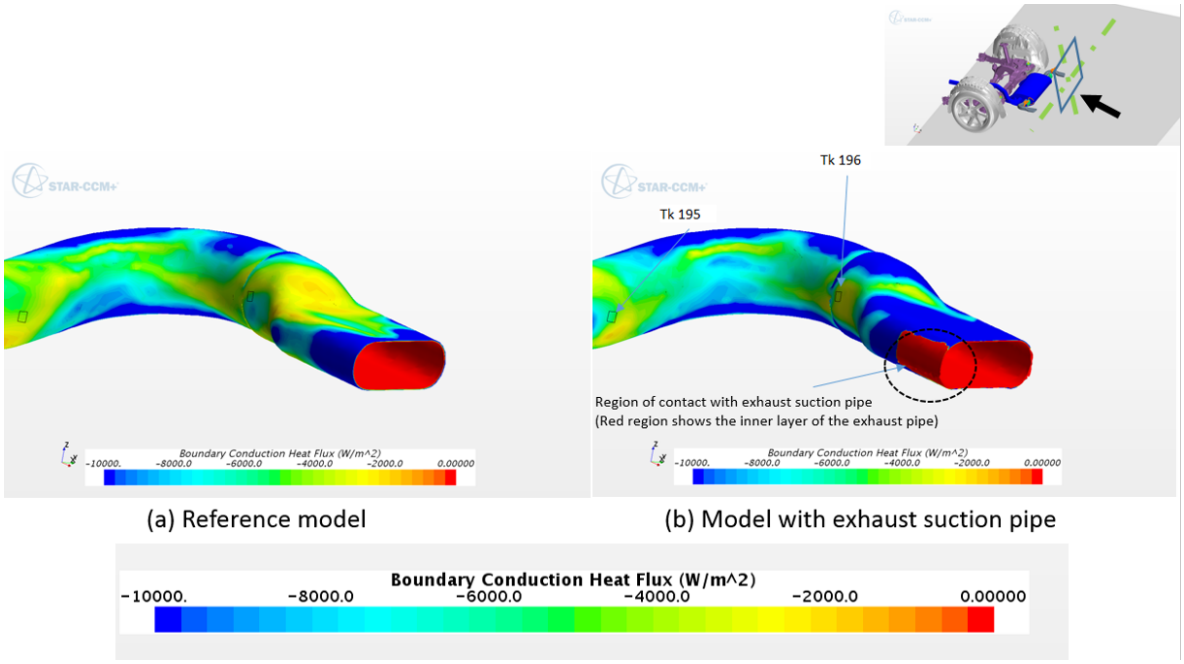

Figure 5-13: Convection comparison of exhaust system between reference model and model with exhaust suction pipes at tk 195 and 196

In addition it is important to note that in this model the exhaust suction pipes are considered as adiabatic walls. Hence the conduction between the mouth of the exhaust suction pipes and the outlet of the exhaust tail pipes are not taken into account even though they are physically in contact to each other as shown in fig 5-2, 5-11 and 5-13. In addition the convective heat transfer of this contact region by the exhaust tail pipe and the metal part of the exhaust suction pipes should have contributed to higher heat transfer. For this reason the decrease in temperature inclusive of this effect will be higher in comparison to the current results.

Heat Shield : It is noticeable that the temperature distribution on rear muffler has changed significantly when compared between the reference simulation model and the simulation model with exhaust suction pipes, similar effect is found in the region of the heat shield close to chamber 'A' of the muffler but the change in temperature for the same models around the region close to chamber 'B' is close to zero, as shown if fig 5-15. The main reason for this can be explained by looking through the upper surface convection of heat shield. The reason for such an occurrence is explained in fig 5-16 showing the convective heat distribution over the heat shield. Although the convective cooling is effective in the regions close to tk 167 and tk 168 which is shown through the fig 5-17, this figure shows the lateral heat shift from left to

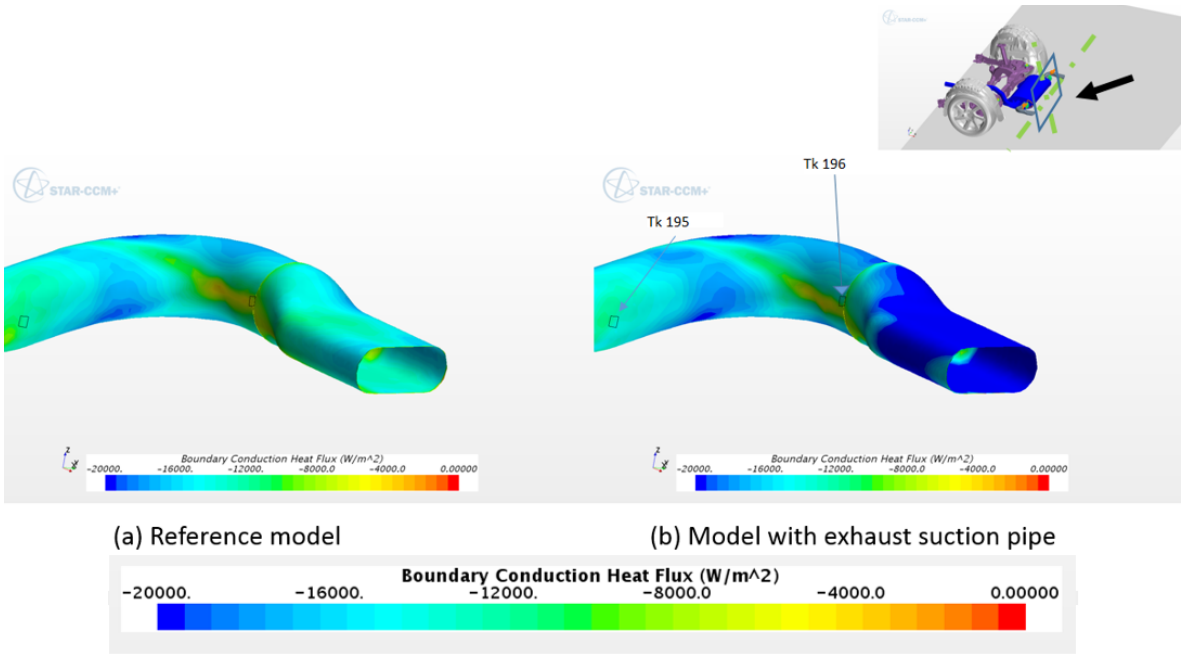

Figure 5-14: Inner surface convection comparison of exhaust system between reference model and model with exhaust suction pipes at tk 195 and 196

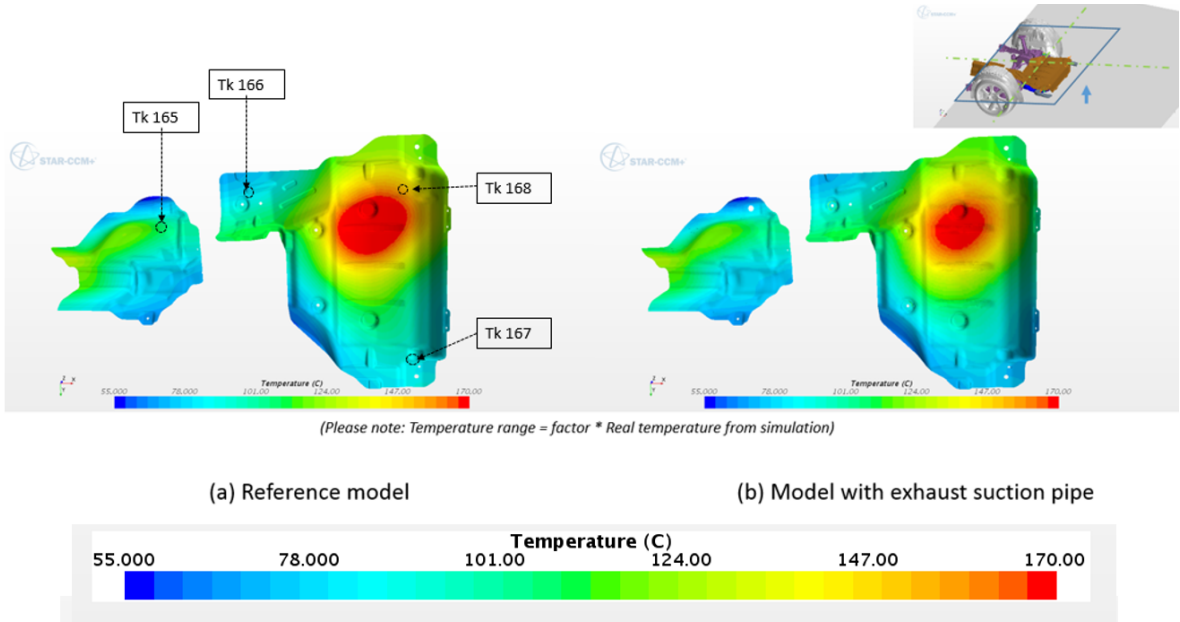

Figure 5-15: Solid temperature comparison of heat shield between reference model and model with exhaust suction pipes (view: lower surface of heat shield)

right which explains the convection pattern found in fig 5-16.

As mention in the above paragraph the temperature deviation on muffler tk points 269 and 194 are high for model with exhaust suction pipes in comparison to reference model. The temperatures of these tk points are very low for the model with exhaust suction pipes. But

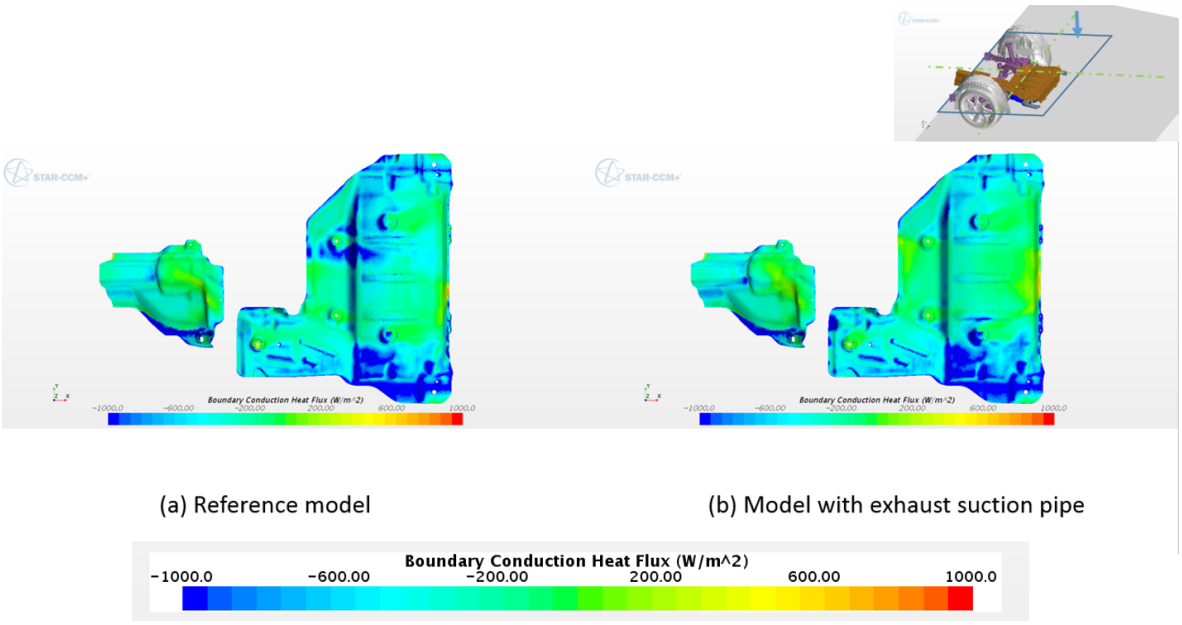

Figure 5-16: Outer convection comparison of heat shield between reference model and model with exhaust suction pipes(view: upper surface of heat shield)

their influence is not observable on the heat shield. Else the decrease in temperature at tk 269 should reduce the temperature of the heat shield close to that region in the same magnitude. This is because the airflow above the heat shield is disturbed in the model with exhaust suction pipes compared to reference model. The flow above the heat shield tends to drift towards the right side due to lower static pressure in right side compared to the left side as shown in fig 5-4. As a result in the upper surface the intense heat found close to tk 168 is shifted towards the right (towards tk 167). Although the intensity of heat doesn't reach till the other end of the heat shield. This hot air drift increases the average temperature of surrounding the heat shield and reduces cooling effect of the heat shield due to poor convection. This heats the middle part of the upper surface of the heat shield creating a hotter surface in the middle. This, along with the conduction of the heat from middle region to through out the heat shield (being made of conductive material), creates a temperature patten close to the reference model temperature pattern.

The cause of such a phenomena is due to the tendency of flow pattern towards right. This is because of the static pressure pressure pattern shown in fig 5-4. The static pressure in overall region underneath the vehicle is lower in this case compared to reference model. However the decrease in static pressure is more in average in the right side of the muffler (when looked from up) compared to the left side. This is due to the presence of exhaust pipe inlet in the left of the muffler unlike right side of the muffler and the suction effect of exhaust suction pipes are more close in the right side of muffler due to asymmetric positioning.

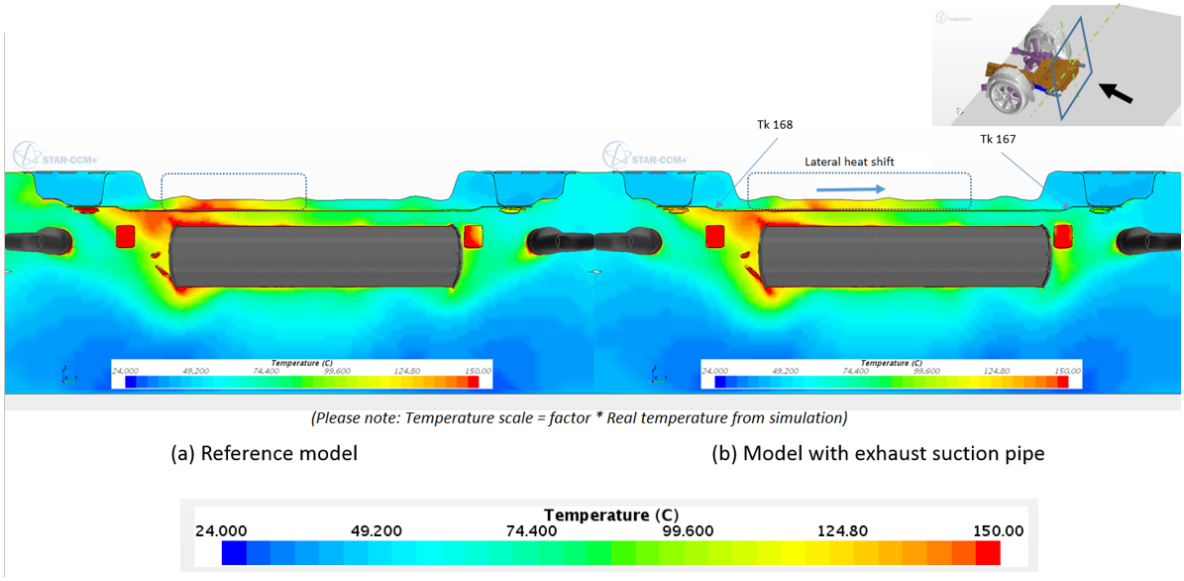

Figure 5-17: Comparison of air temperature surrounding heat shield between reference model and model with exhaust suction pipes at tk 167 and 168 along YZ plane

5-2 Conclusion

The influence of the exhaust suction pipe on thermal simulation is quantified. Among the other parameters of study this one highlights itself by bringing a notable temperature deviation. However it is clear from the fig 5-3 that its influence only remain in the rear end of the vehicle. There is no influence due this suction effect in the tk points close to the front half of the vehicle, such as tk 221 and 222. It is important to note that the deviation is totally dependent on how the suction pipe is attached to the exhaust tail pipe as different attachments result in different leakage ratio. In some cases only one suction pipe will be attached, i.e for vehicles with only one tail pipe, which also changes the leakage ratio. Moreover it is dependent on the inner geometry of the rear muffler. Since the muffler geometries vary from one model to another the scale of temperature deviation observed here is only specific to this model. To explain in detail, say the given muffler geometry has the exhaust inlet pipe connected directly to the center chamber unlike this model where it is connected to the left chamber ('A'). The decrease in temperature at tk 269 and 194 will not be so high. In addition the flow nature (the stagnant region) close to tk 191 will be different. The interesting result from this simulation is that the simulation readings are closer to experimental values which explains the importance of including the exhaust suction pipes while designing wind-tunnel modelling. The results obtained can be more accurate when correlated with experimental values provided the simulation runs with a much more finer mesh.

Chapter 6

Simulation of Model with Reduced Ride Height

Being one of the parameters under study variation in ride height is looked into using two models. The first model is with normal ride height, $160mm$ (reference model) and second model with lower ride height, $110mm$ giving a reduction of ride height by $50mm$, as shown in figure 6-1. The increase in velocity with decrease in ride height plays the major role over the trend of decrease in temperature throughout the model. As a result the convective heat transfer is higher for lower ride height. Table shown in fig 6-2 shows the temperature deviation due this change. It is clear that the deviation trend is negative, i.e, the temperature has decreased with reduced ride height.

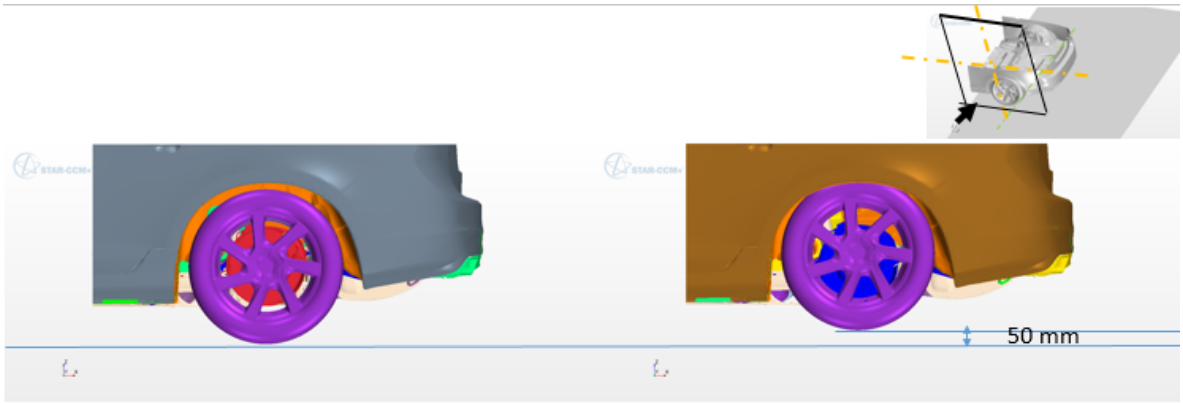

(a) Reference model

(b) Model with reduced ride height

Figure 6-1: Ride height comparison between the two models

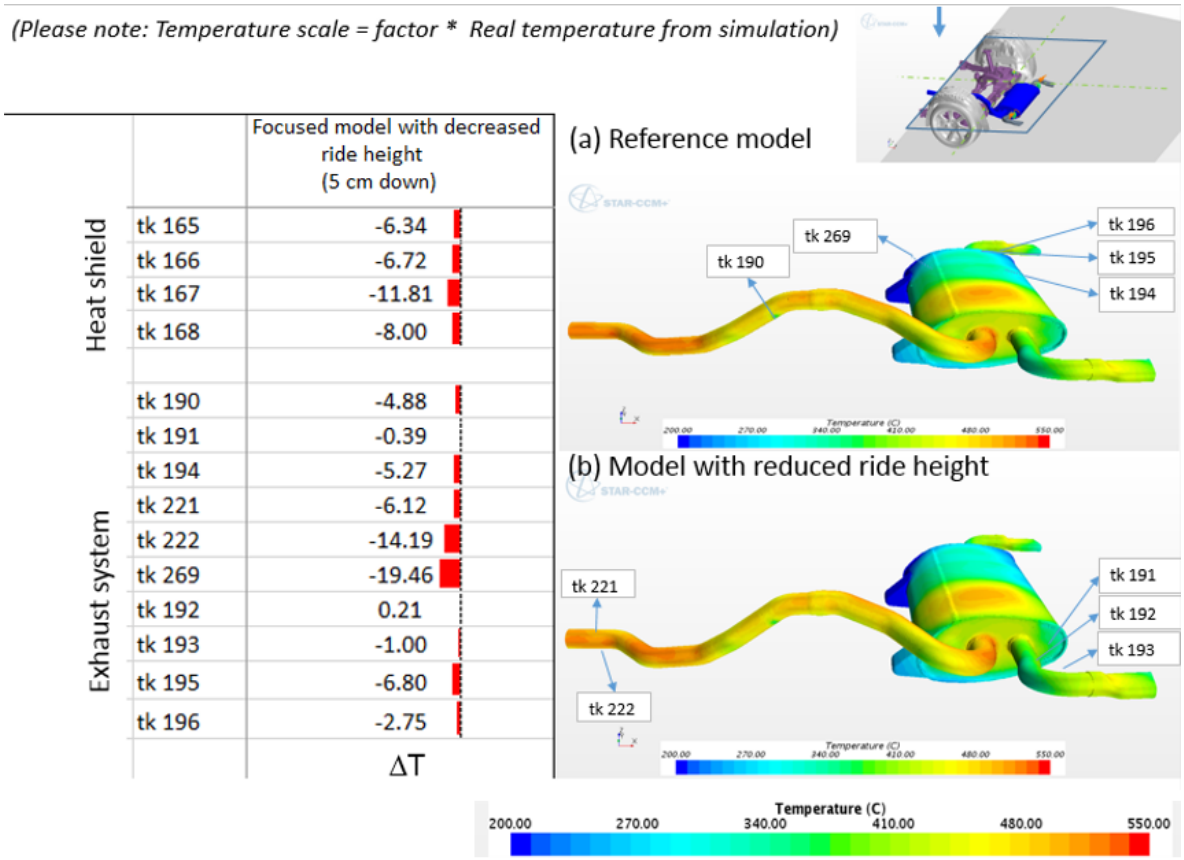

Figure 6-2: Table of temperature deviation between reference model and model with reduced ride height at vehicle velocity = $70\frac{km}{h}$. The temperature deviation ΔT = Temperature reading of model with reduced ride height - Temperature reading of reference model

6-1 Detailed Observation and reasoning

Since the trend of temperature deviation (decrease in temperature) is similar for all tk points, the reasoning for their occurrence is almost identical. Some of the significant tk points are explained in detail.

The stagnant flow found on the left upper surface close to tk 165 and 166 changes to a flow with notable velocity magnitude. Moreover the average velocity surrounding this region has increased in the model with decreased ride height as shown in the velocity distribution of a YZ plane cut along tk 166, fig 6-3. The heat shields are heated up primarily by the radiative heat transfer from the exhaust system. Since the flow close to the exhaust pipe is higher there is more convection, resulting in decrease in exhaust pipe temperature. This directly reduces the radiation emitted by the exhaust pipes resulting in lower radiation heat transfer to the heat shields. This is occurrence is visible from table shown in fig 6-2. Take tk 190 which is positioned on the exhaust pipe is close to tk 166 for example. There is a decrease in temperature by 5 degrees in tk 190 which plays a major role in the decrease in temperature for tk 166.

In addition, the temperature gradient of air from the exhaust pipe to the heat shield along the

z axis (vertical) has increased as shown in fig 6-3. This is due to the increased velocity gradient along x axis. As a result the air surrounding the heat shield is cooler in this simulation model compared to reference model. This enhances convective heat transfer. In the reference model the heat shield is hotter in the left side compared to the model with reduced ride height as pointed out in fig 6-4. More dominantly there is an effective convective cooling on the right side which acts like a fin.

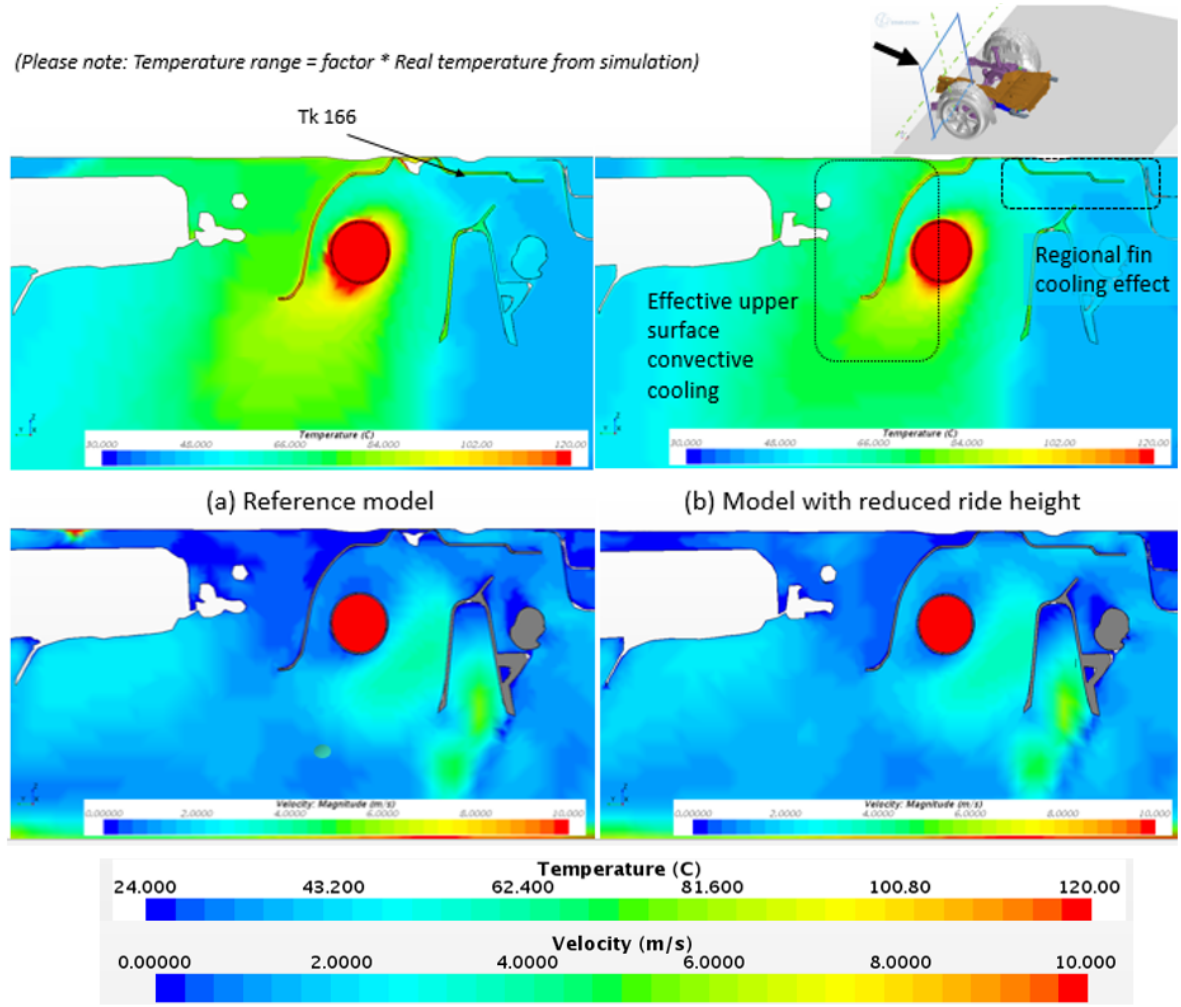

Figure 6-3: Comparison of air temperature and velocity surrounding the heat shield between reference model and model with reduced ride height at tk 166 along YZ axis

When it comes to the influence over the rear part of muffler heat shield consisting of tk 167 and 168, the contributor to the temperature deviation (decrease in temperature) is the rise in flow velocity magnitude between the muffler and muffler heat shield as pointed out by fig 6-5. When looked into the convection over the heat shield, fig 6-6, it is clear that the increase in velocity along x direction has decreased the heating of the heat shield through vertical convection from the heat source, i.e muffler. The fig 6-5 makes it easier to visually analyse this occurrence.

Fig 6-7 shows that the temperature of air circulating close to tk points 194 and 269 are

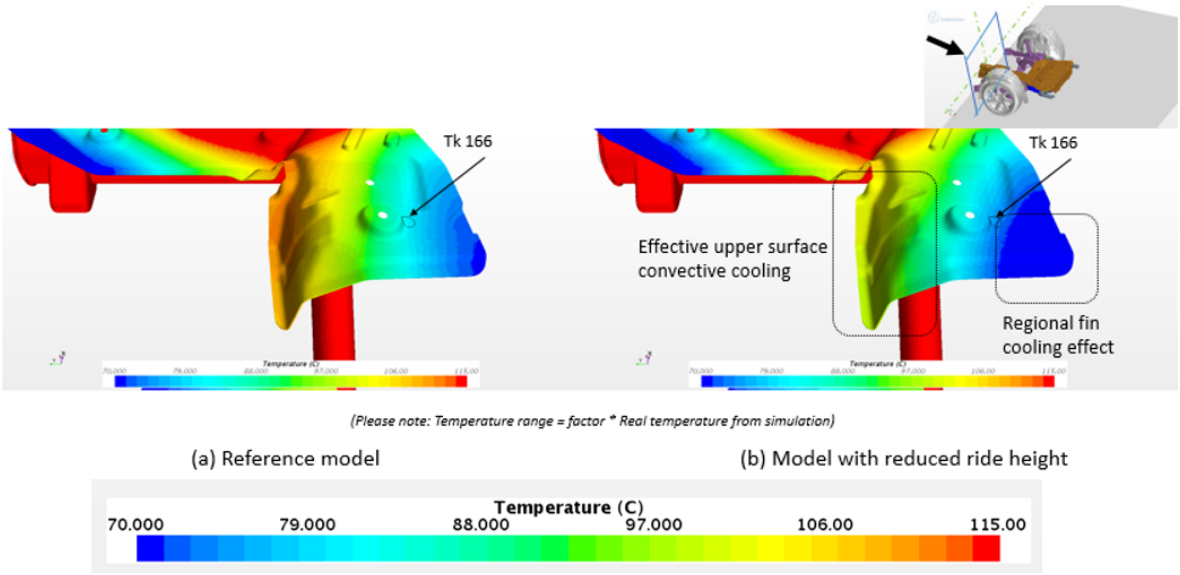

Figure 6-4: Comparison of solid temperature of the heat shield between reference model and model with reduced ride height at tk 166

lower in this case compared to reference model. Fig 6-8 and 6-9 reason this fact by showing the increase in velocity of air flowing close to the walls of muffler and the resulting average increase in convection along the side of muffler having the tk points 194 and 269.

The deviation is higher in the right side of the muffler compared to left side as it is clear from the readings from tk 269 and 194 compared to the left side. This is due to smoother flow of air along the right side. Since the muffler is placed slightly offset towards right from the central axis, the air flows with lower hindrance from the rear exterior of the vehicle. The flow along the left side of the muffler is hindered from the beginning due to the exhaust inlet pipe attached to it. The significant hindrance of rear exterior of the vehicle and the inlet exhaust pipe to the muffler minimizes the flow velocity locally along the left side of the muffler, hence minimizing the heat convection.

6-2 Conclusion

Variation of ride height has a steady trend with respect to the temperature deviation throughout the vehicle. Unlike the other parameters, this one has influence throughout the complete vehicle (from the front to rear of the vehicle). The deviation of temperature versus ride height cannot be concluded to be linear. However, it is obvious that a decrease in ride height leads to decrease in temperature and vice versa. The reduction in ride height has improved the suction effect underneath the vehicle. Such a phenomena is called the ground effect. When it comes to comparison between the CAD model and the real model, there is a possibility of variation of ride height. For example the provided CAD model is designed with three persons in the vehicle while the experimental model will have no person inside. However there will be few heavy equipments on board that can increase the weight of the empty vehicle. Hence it is important to determine the added weight and input the relative ride height in CAD model

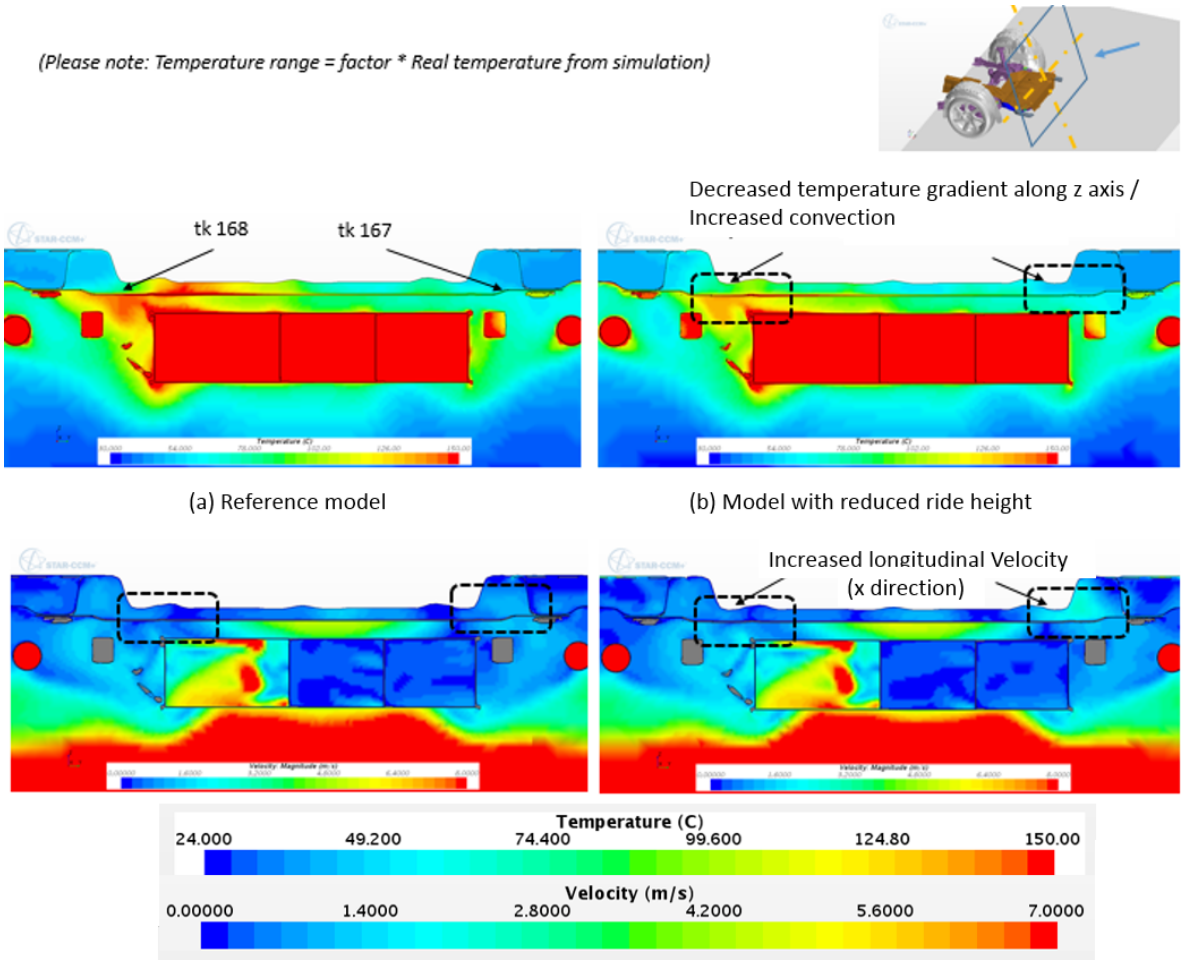

Figure 6-5: Comparison of air temperature and velocity surrounding the heat shield between reference model and model with reduced ride height at tk 167 and 168 along YZ axis

for computational simulations. Hence when it comes to simulating the model, it should be a factor of concern in order to bring out an accurate correlation with experiments.

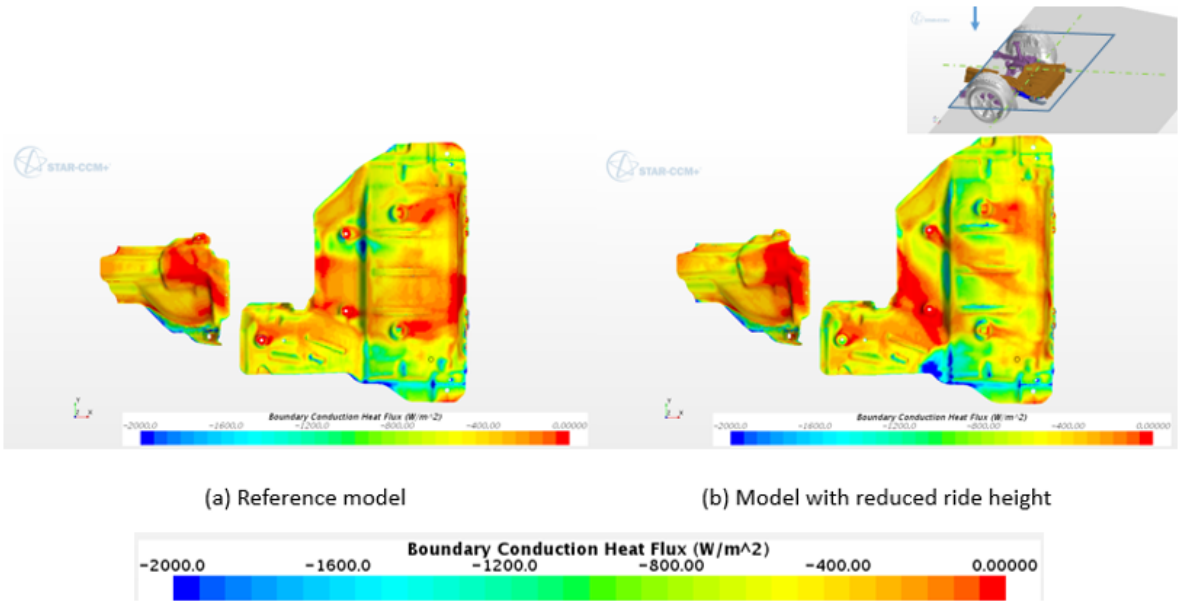

Figure 6-6: Comparison of convection of the heat shield between reference model and model with reduced ride height at tk 166 and 168

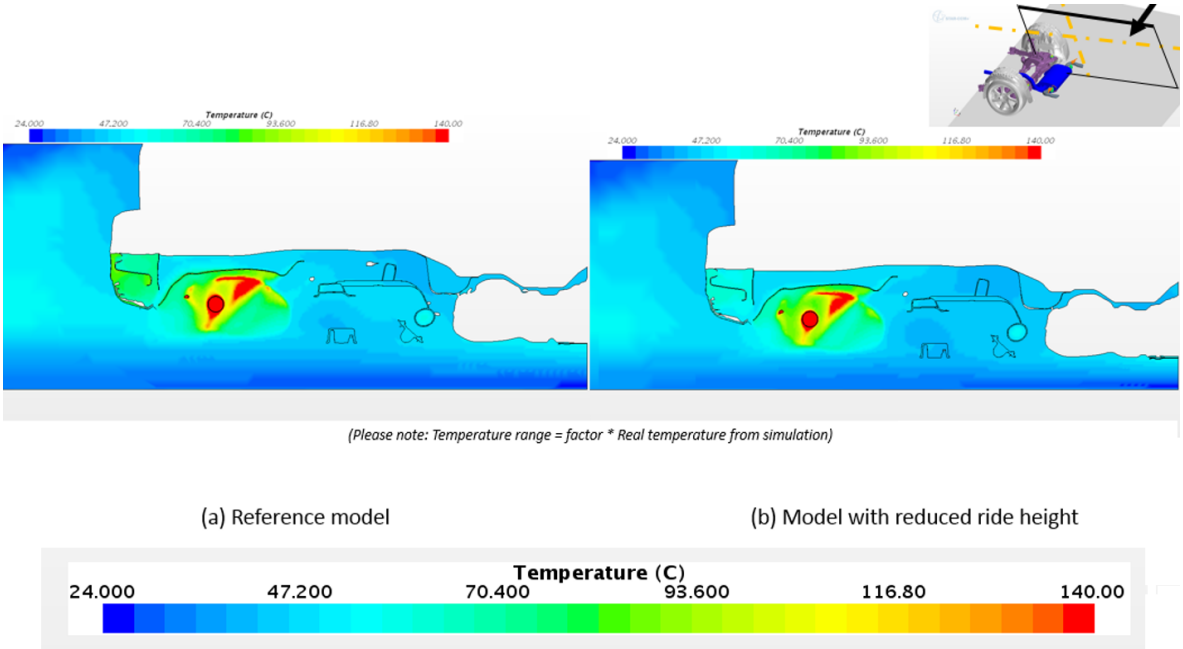

Figure 6-7: Comparison of air temperature surrounding the exhaust system between reference model and model with reduced ride height at tk 194 and 269 along XZ axis

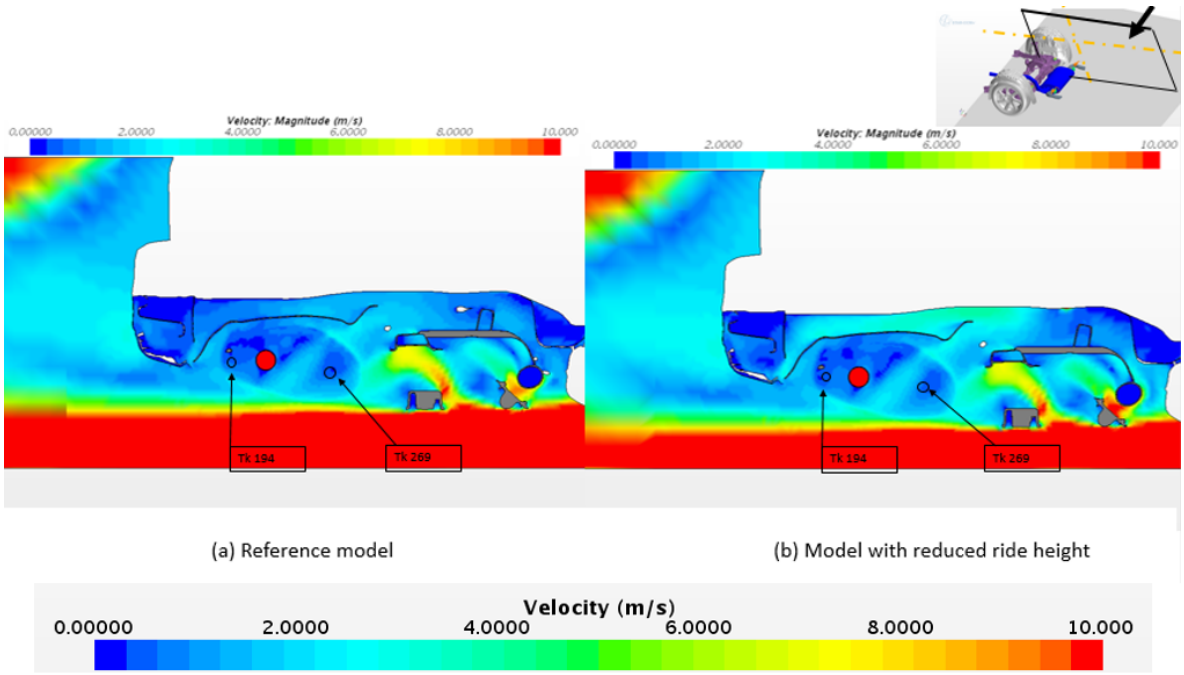

Figure 6-8: Comparison of air velocity surrounding the exhaust system between reference model and model with reduced ride height at tk 194 and 269 along XZ axis

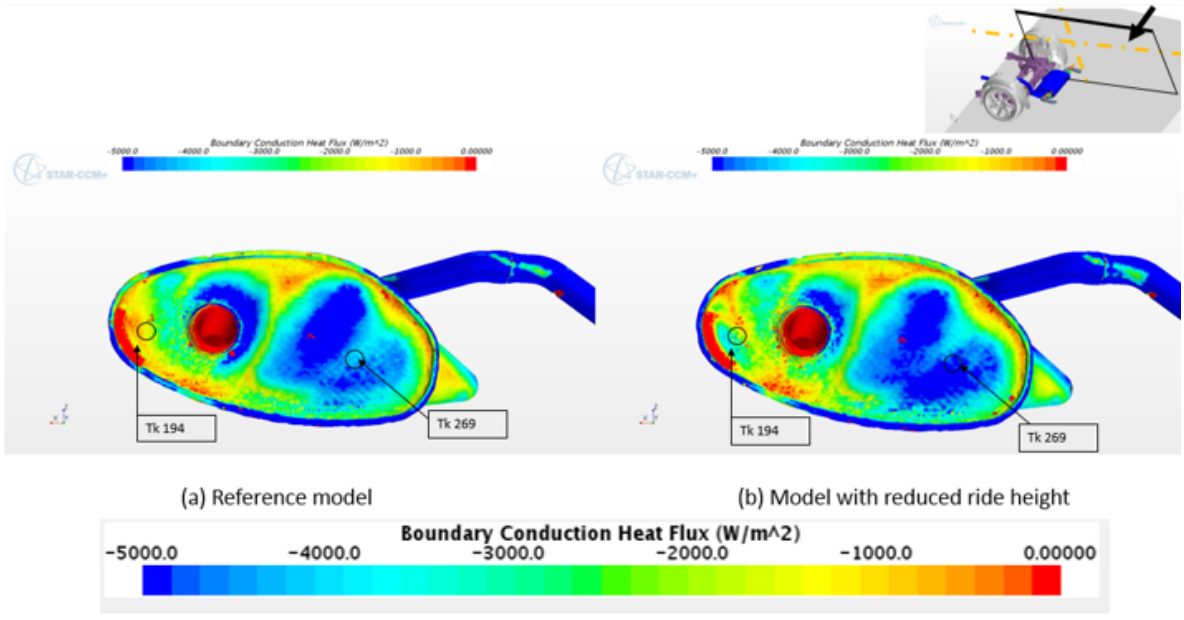

Figure 6-9: Comparison of convection of the exhaust system between reference model and model with reduced ride height at tk 194 and 269

Chapter 7

Discussion, Conclusion and Future Research

7-1 Limitations of The Simulation Models

The model used for simulation has many advantages such as simplicity, reduced time consumption, acceptable results for detailed study among others. However such a model comes with some disadvantages as well.

Firstly, in the focused domain, the boundary conditions are taken from an already developed full model simulation without exhaust suction pipes. This increases the accuracy of boundary conditions. These boundary conditions include inlet region, top region and sides. The outlet boundary condition cannot be traced from the full model simulation because unlike full model simulation this model has two exhaust suction pipes. Also in the model, the exhaust suction pipes are not completely contained in the domain. Since the pipes protrude out of the domain, the only option available is to keep the outlet boundary condition at constant pressure, given as $1.1 * 10^5 Pa$ absolute total pressure condition. It is common to put outlet boundary condition as constant pressure in a wind tunnel simulation, but in those cases the outlet is far beyond the domain of study giving ideally zero effect on the domain under study. In this case the domain is quite small and providing such a pressure boundary condition will have an effect on the flow upstream. As a consequence the values could be slightly deviated from that found from a full car and wind tunnel simulation results. In addition the influence of blockage due to the pipe is not involved in this model. Fig 7-1 clearly explains the concept mentioned in this paragraph.

Secondly, the growth rate of cells are kept high for building a relatively coarse volume mesh. This results in a less refined flow profile prediction underneath the vehicle. It will capture a good boundary layer flow profile but flow profile as a whole between the under-skin of vehicle to the floor is inaccurate. To improve the capturing quality of the flow pattern, the cells

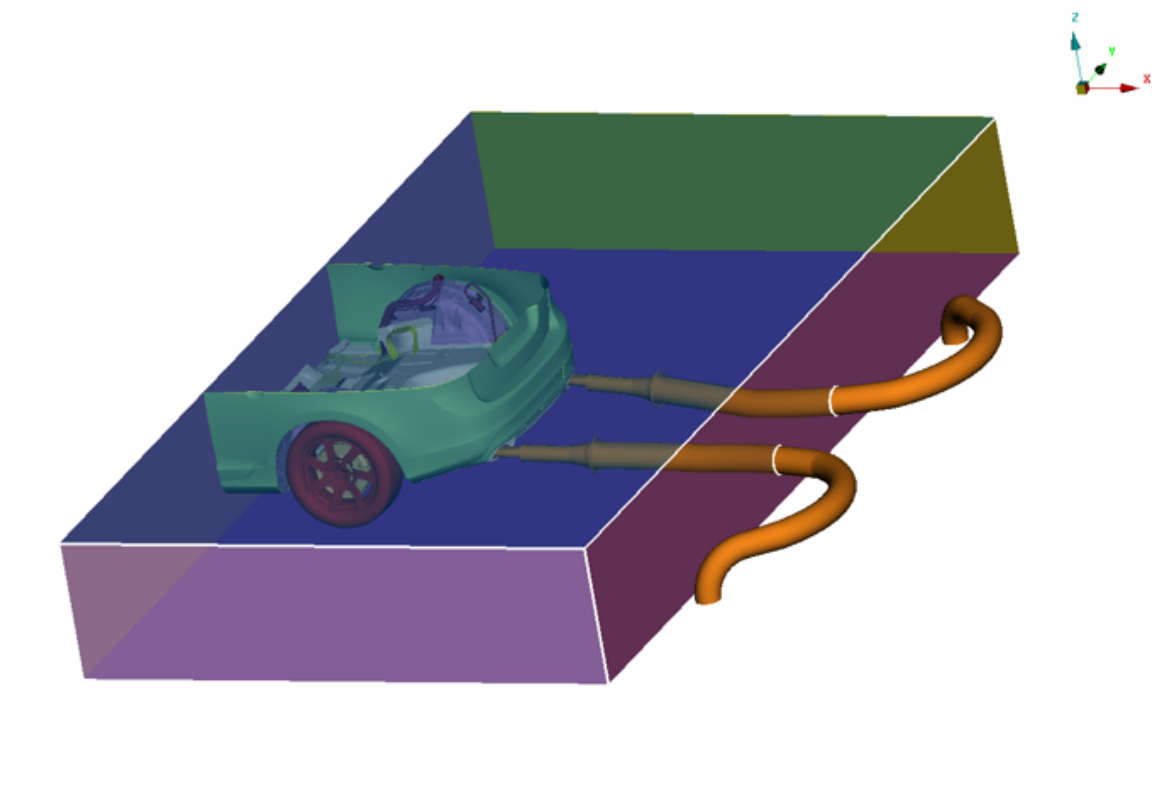

Figure 7-1: The constrained domain

underneath the vehicle should be more refined.

Thirdly, due to different mesh demands between different parts, it is difficult to interpolate over the interface between these parts. This will lead to unsatisfactory impractical results. However since these cells are limited to small regime in these thesis models, their effects are limited when it comes to transfer of their information to neighbouring cells.

Fourthly, use of RANS is not the best option when it comes to analysing the flow inside complex geometries such as inside muffler. This is because in physical testing the flow inside the exhaust system is not steady hence eddies and vortices of high energy and small scales will not be highlighted through this method. RANS is preferred in industries due to cost and time management over accuracy. In order to capture more accurate flow physics inside the muffler Large eddy simulation (LES) or Detached eddy simulation (DES) should be used.

Finally, in chapter 4, the exhuast suction pipes are considered as adiabatic walls, as a result the conduction between the mouth of the exhaust suction pipes and the outlet of the exhaust tail pipes are not taken into account even though they are physically in contact with each other. It is described in detail in section 5-1 and shown in fig 5-2, 5-11 and 5-13. In addition the convective heat transfer of this contact point and the metal part of the exhaust suction pipes should have contributed to higher heat transfer. Thus the decrease in temperature

inclusive of this effect will be higher in comparison to the current results.

7-2 Conclusion

Research justifies how important it is to implement the influences of factors included in virtual wind-tunnel modelling. As the Volvo Environment and Fluid engineering is eagerly looking forward towards an accurate and robust Virtual Wind Tunnel Simulation model it is obvious to have correlation among results of different departments. In this research four parameters are investigated. They are:

1. *Exhaust Suction Pipes:* It has the most profound influence among the other parameters that were investigated. This is because, unlike other parameters it affects the flow inside the muffler. However its influence is limited to the rear half of the vehicle especially, on the exhaust system and the heat shields. This parameter gave an interesting result. The temperature readings from the simulation has a closer match with the experimental readings compared to readings from a full model simulation without this parameter. A finer meshing of the domain will improve the flow physics and result in a more accurate correlation to the experimental readings. It should be noted that the effect of flow inside the muffler is dependent on the internal geometry of the muffler. Also the accuracy of the result depends on the suction leakage factor. For different exhaust tail pipes, the connecting tubes to the suction pipes are different creating different blockage ratio. Hence different attachments have different suction leakages. This should be taken into account while simulating or modelling the geometry. Some vehicles will have only one exhaust pipe. In that case although the trend of the temperature will be negative (i.e, decreased temperature reading compered to reference model) the variation pattern of this deviation differ from the study above.

2. *Wheel Rotation and MRF on Rims:* The involvement of both MRF on rims and wheel rotation were studied. It can be observed that the wheel rotation has an overall impact on the rear of the vehicle, notably on exhaust system and heat shields. MRF on rims has a notable impact on the flow pattern underneath the vehicle. But the impact of MRF on rims is region specific but vivid. In the current model, influence of MRF is shown only in two tk points but the magnitude of temperature deviation is twice that of the model with only wheel rotation. So the involvement of MRF on rims depend on the additional time consumed over the gain in accuracy of temperature prediction. However the time consumed by MRF is quite small hence it is only the matter of additional settings required for preparing the MRF approach.

   It is important to understand that the influence of wheel rotation for a given wheel size and ride height will have the same trend with respect to temperature deviation as tabulated in this work. However the influence of MRF on rims will change in relation to the rim profile. The rim profile studied here showed a slight inward suction effect hence the influence is regional. The range of its impact is depended on the rim profile. Thus different rim profiles provide different deviation in temperatures at different regions. A further research on these profiles is necessary to provide a better conclusion. Observing the temperature deviations along the tk points, it is clear that the influence of both these factors included in the rear wheels lie only in the rear half of the vehicle.

3. *Ride Height:* The deviation of temperature is observed from the beginning of the exhaust system in the domain which suggests that the variation of ride height influences the entire vehicle. The decrease in temperature observed in this model is due to the phenomena called as ground effect. The reduction in ride height has improved the suction effect underneath the vehicle. Usually a common CAD model is used for computational simulations depicting wind tunnel simulations. This will give way to errors due to variation in ride height. In the model in this research work an exaggerated decrease of ride height of $50mm$ is considered. The main focus being to clearly demonstrated its influence on temperature readings has been successfully tabulated. Thus when it comes to factor of concern the variation of ride height with respect to experimental ride height should be first noted. If the difference is significant then this element should be considered as the factor of influence.

Finally this observation and investigation will help in integrated Virtual Wind Tunnel simulations with an acceptable correlation in individuals' results. This will benchmark the potential elements in wind-tunnel modelling that will affect the simulation results as far as thermodynamic simulation is concerned, providing a wider opportunity towards different possible investigations for future research. It will place the accuracy standards of the thermal simulation to that of other departments when it comes to wind-tunnel modelling. Finally and most importantly, it will be a benchmark for future development in Virtual Wind Tunnel Design project from thermal perspective.

7-3 Future Research

The conclusions from this work provides potential ground work for future research topics.

- Design and development of exhaust suction pipes: Since this element plays major role in the accuracy of thermal simulation results to that of experimental results it is important to design and develop an exhaust suction pipe that will influence the experimental simulations to a lower extent. This will bridge the gap between the real road conditions and physical wind tunnel test results. The design and development includes minimized suction influence inside the exhaust muffler, lower suction leakages, minimize the deviation of the effect for having single exhaust tail pipe and dual tail pipes.

- Optimizing current exhaust suction pipes: Optimizing the current exhaust pipe and modifying the attachment section of the suction pipe to that of the end of exhaust tail pipe. Finding a universal attachment geometry will minimize the variation of suction leakage for different exhaust tail pipe geometries.

- Detailed study of various rim profiles: The importance of wheel rotation is clear from this thesis. But the influence of different rim profiles should be studied in detail. As mentioned in the conclusion of section 6-2, different profiles show different characteristics. Also, depending on the complexity of the rim profiles, a detailed research relating the accuracy of MRF approach over sliding mesh approach will be a valuable addition to this topic.

- MRF on front rims: As explained in section 7-2, the impact of MRF on rear rims for the given rim profile is negligible. But the impact by the MRF on front rims located near the engine bay may differ. Unlike the rear, the engine bay is tightly packed with pre-determined complex air flow paths. Hence the possibility of influence due to slightest variation in the flow pattern as a consequence of MRF on front rims cannot be neglected.
- Full model simulation: Since the model under study is comparatively small, a full model simulation is necessary to conclude the influence with more accuracy. Since the domain is small in this research the influence due to blockage factor of the exhaust suction pipe is not quantified. In addition since this model is relatively coarser than normal full model simulation, the flow physics captured by the simulation will be less accurate.
- Exhaust suction effect on different muffler geometries: Mufflers are of many different sizes and with different inner geometries. Different mufflers are attached to these vehicles depending on related specifications. Hence it is important to study and note the final outcome of temperature distribution and exhaust inner flows due to suction effect in these different mufflers.

Bibliography

[1] M. Khaled, M. Ramadan, H. El-Hage, A. Elmarakbi, F. Harambat, and H. Peerhossaini, "Review of underhood aerothermal management: Towards vehicle simplified models," *Applied Thermal Engineering*, vol. 73, pp. 842–858, 2014.

[2] A. Alajbegovic, R. Sengupta, and W. Jansen, "Cooling airflow simulation for passenger cars using detailed underhood geometry, in: SAE World Congress," *SAE Technical Paper 2006-01-3478.*, 2006.

[3] V. Kumar, S. Kapoor, G. Arora, and S. Saha, "A combined cfd and flow network modeling approach for vehicle underhood air flow and thermal analysis, in: SAE World Congress," *SAE Technical Paper 2009-01-1150*, 2014.

[4] D. Baeder, T. Indinger, N. Adams, and F. Decker, "Comparison of numerical simulations with experiments of bluff bodies including under-hood flow, in: SAE World Congress, year = 2011, journal = SAE Technical Paper 2011-01-0171„"

[5] M. Khaled, A. Al Shaer, F. Hachem, F. Harambat, and H. Peerhossaini, "Effects of ground vehicle inclination on underhood compartment cooling," *Automotive technology*, vol. 13, 2012.

[6] T. J. Bender, "Commissioning report: PVT Ground Simulation Upgrade," Confidential report with in Volvo*, December*, 2006.

[7] C. Landstrom, T. Walker, and L. Lofdahl, "Detailed flow studies in close proximity of rotating wheels on a passenger car, SAE World Congress," *SAE Technical Paper 2009-01-0778*, 2009.

[8] C. Landstrom, T. Walker, and L. Lofdahl, "Effects of ground simulation on the aerodynamic coefficients of a production car in yaw conditions, SAE World Congress," *SAE Technical Paper 2010-01-0755*, 2010.

[9] C. Landstrom, S. Sebben, and L. Lofdahl, "Effects of wheel orientation on predicted flow field and forces when modelling rotating wheels using CFD, 8th MIRA International Vehicle Aerodynamics Conference "Low Carbon Vehicles", UK," 2010.

[10] Y. Cengel and A. Ghajar, "Heat and mass transfer: Fundamentals and applications, isbn-13: 978-0077366643," *McGraw-Hill*, vol. 4rd, 2011.

[11] R. Siegel and J. Howell, "Thermal radiation heat transfer," *Hemisphere Publishing Co.*, vol. 3rd, 1992.

[12] B. Munson, A. Rothmayer, T. Okiishi, and W. Huebsch, "Fundamentals of fluid mechanics," *ISBN-13: 978-1118399712*, vol. 7th, 2015.

[13] L. Leob, *The Kinetic Theory of Gases*, vol. 3rd edition. Dover Publications Inc.

[14] CD-adapco, *STAR-CCM+ User Guide> Modeling Physics> Modeling Flow and Energy> The Coupled Flow Model*. STAR-CCM+ Documentation, Version 11.02.

[15] B. Daly and F. Harlow, "Transport equations of turbulence," *Physics of Fluids 13, pp. 2634-2649*, 1970.

[16] W. Rodi, "Experience with two-layer models combining the k-e model with a one-equation model near the wall," *29th Aerospace Sciences Meeting, January 7-10, Reno, NV, AIAA 91-0216.*, 1991.

[17] R. Henkes, F. van der Flugt, and C. Hoohendoorn, "Natural convection in a square cavity calculated with low-reynolds number turbulence models," *International Journal of Heat and Mass Transfer, 34, pp. 1543-1557.*, 1991.

[18] W. Jones and B. Launder, "The prediction of laminarization with a two-equation model of turbulence," *International Journal of Heat and Mass Transfer, 15, pp. 301-314.*, 1972.

[19] T.-H. Shih, W. Liou, A. Shabbir, Z. Yang, and J. Zhu, "A new $k-\epsilon$ eddy viscosity model for high reynolds number turbulent flows - model development and validation," *NASA TM 106721.*, 1994.

[20] W. Reynolds, "Fundamentals of turbulence for turbulence modeling and simulation," *Standford University CA Dept. of Mechanical Engineering*, 1987.

[21] S. Salim and S. Cheah, "Wall y^+ strategy for dealing with wall-bounded turbulent flows," *Proceedings of the International MultiConference of Engineers and Computer Scientists 2009 IMECS, Hong Kong*, vol. 2, 2009.

[22] E. Kos, "Which y+ should i choose for which turbulence model?." http://www.steve.cd-adapco.com, last visited on on 9/26/2014, 2016.

[23] M. F. Modest, "Radiative heat transfer," *Academic Press*, vol. Second Edition, 2003.

[24] R. Taylor and R. Luck, "Comparison of reciprocity and closure enforcement methods for radiation view factors," *Thermophysics and Heat Transfer*, vol. 9:4, pp. 660-666, 1995.

[25] J. Holman, "Heat transfer," *Eighth SI Metric Edition, McGraw Hill*, 2001.

[26] P. Gullberg, L. Löfdahl, S. Adelman, and P. Nilsson, "A correction method for stationary fan cfd mrf models, sae technical paper 2009-01-0178," *doi:10.4271/2009-01-0178*, 2009.

[27] P. Gullberg, L. Löfdahl, P. Nilsson, and S. Adelman, "Continued study of the error and consistency of fan cfd mrf models, sae technical paper 2010-01-0553," *doi:10.4271/2010-01-0553*, 2010.

[28] P. Gullberg and R. Sengupta, "Axial fan performance predictions in cfd, comparison of mrf and sliding mesh with experiments, sae technical paper 2011-01-0652," *doi:10.4271/2011-01-0652*, 2011.

[29] CD-adapco, *STAR-CCM+ User Guide> Meshing> Volume Meshing.* STAR-CCM+ Documentation, Version 11.02, CD-adapco.

[30] A. Cogotti, "Flow field of an isolated rotating wheel. Preliminary results. ECARA Ground Simulation Committee, FKFS, Stuttgart," *ppt presentation only*, 10 October 2001.

[31] C. Landstrom, L. Christoffersen, T. Walker, and L. Lofdahl, "Influences of different front and rear wheel designs on aerodynamic drag of a sedan type passenger car, SAE World Congress," *SAE Technical Paper 2011-01-0165*, 2011.